FORM T1-12
8/94

WAPD-T-3149

HYDROGEN EMBRITTLEMENT, GRAIN BOUNDARY SEGREGATION AND STRESS CORROSION CRACKING OF ALLOY X-750 IN LOW AND HIGH TEMPERATURE WATER

W. J. Mills, M. R. Lebo and J. J. Kearns

April 1997

U. S. Department of Energy Contract DE-AC11-93PN38195

BETTIS ATOMIC POWER LABORATORY WEST MIFFLIN, PENNSYLVANIA 15122-0079

Operated for the U. S. Department of Energy
by WESTINGHOUSE ELECTRIC CORPORATION

THIS PAGE IS INTENTIONALLY BLANK

HYDROGEN EMBRITTLEMENT, GRAIN BOUNDARY SEGREGATION AND STRESS CORROSION CRACKING OF ALLOY X-750 IN LOW AND HIGH TEMPERATURE WATER

ABSTRACT

The nature of intergranular stress corrosion cracking (SCC) of Alloy X-750 was characterized in low and high temperature water by testing as-notched and precracked fracture mechanics specimens. Materials given the AH, BH and HTH heat treatments were studied. While all heat treatments were susceptible to rapid low temperature crack propagation (LTCP) below 150°C, Conditions AH and BH were particularly susceptible. Low temperature tests under various loading conditions (e.g., constant displacement, constant load and increasing load) revealed that the maximum stress intensity factors (K_{Pmax}) from conventional rising load tests provide conservative estimates of the critical loading conditions in highly susceptible heats, regardless of the load path history. For resistant heats, K_{Pmax} provides a reasonable, but not necessarily conservative, estimate of the critical stress intensity factor (K_I) for LTCP. Testing of as-notched specimens showed that LTCP will not initiate at a smooth surface or notch, but if a crack-like defect is present it readily occurs. Comparison of the cracking response in water with that for hydrogen-precharged specimens tested in air demonstrated that LTCP is associated with embrittlement of grain boundaries by hydrogen generated by the corrosion reaction at the crack tip. Equivalent activation energies for Stage II LTCP rates (11.3 kcal/mol) and hydrogen diffusion (11.5 kcal/mol) indicate that hydrogen diffusion to the peak stress regions ahead of a crack is the rate controlling process. Auger analysis showed that heat treatment and heat-to-heat variability was associated with phosphorus and sulfur segregation to grain boundaries. Above 150°C, rapid cracking does not occur due to an increase in fracture resistance and decrease in the degree of hydrogen enrichment. SCC initiation and growth does occur in high temperature water (>250°C), but crack growth rates are orders of magnitude lower than LTCP rates. The SCC resistance of HTH heats was far superior to that for AH heats as crack initiation times were two to three orders of magnitude greater and growth rates were one to two orders of magnitude lower.

(PMT)208-WJM
February 18, 1997

TABLE OF SYMBOLS

a	crack length
A	coefficient in Arrhenius crack growth rate relationship
CMOD	crack mouth opening displacement
C	local concentration of hydrogen
C_o	bulk concentration of hydrogen
C_s	surface concentration of hydrogen
D	diffusion coefficient for hydrogen
da/dt	crack growth rate
J_{IC}	elastic-plastic fracture toughness in air
K_I	stress intensity factor
K_{Pmax}	K_I value at maximum load in rising load (i.e., increasing displacement) tests
$K_{ISCC\text{-}LT}$	critical K_I level below which rapid low temperature crack propagation does not occur
K_{JC}	critical stress intensity factor computed from J_{IC}
K_t	theoretical stress concentration factor
$\dot{K}$	stress intensity factor rate during rising load tests
n	stress exponent in power-law relationship correlating crack initiation time with PSES
PSES	peak surface elastic stress (PSES = $K_t \cdot \sigma$)
Q_{INC}	activation energy for incubation of high temperature SCC from a precrack
Q_{LTCP}	activation energy for Stage II crack growth rates at low temperature
Q_{SCC}	activation energy for crack growth rates at high temperature
R	universal gas constant
t	time
$t_{1/2Pmax}$	time required to go from maximum load to one-half maximum load (during rising load test)
t_{INC}	time required to incubate high temperature SCC from a precrack
t_{INI}	time required to initiate high temperature SCC at a notch
T	absolute temperature
$\overline{V}$	partial molar volume of hydrogen in solution
W	width of compact tension specimen
x	distance from surface
σ	nominal stress
σ_H	hydrostatic stress
σ_{YY}	maximum principal stress ahead of a crack
σ_{YS}	yield strength
ρ	root radius of notch tip

INTRODUCTION

Alloy X-750 is a precipitation hardened nickel-base superalloy that is used in high strength fastener applications because of its high temperature strength, corrosion resistance and load relaxation resistance. Studies have shown that this material is susceptible to intergranular stress corrosion cracking (SCC) in low temperature (<150°C) and high temperature (>250°C) water.[1-3] Moreover, evidence of SCC in Alloy X-750 components has been observed in light water reactors.[4-6]

Alloy X-750 is a very mature alloy system having undergone a significant evolution involving heat treatment, chemistry and processing changes aimed at improving SCC properties. Variations in heat treatment have the greatest effect on SCC performance, and the most common heat treatments for fasteners, termed Conditions AH, BH and HTH, are given in Table 1. The original fastener materials were given the Condition AH treatment, but this resulted in inferior SCC initiation and crack growth properties at high temperatures and variable cracking resistance at low temperatures. While the Condition BH treatment improved high temperature SCC (HTSCC) properties, it resulted in a high degree of variability[1] and rather poor low temperature crack propagation (LTCP) resistance.[7] The Condition HTH treatment improved SCC performance at both high and low temperatures and reduced heat-to-heat variability. The 1093°C anneal resulted in a uniform microstructure, substantial grain growth and a lower yield strength relative to Condition BH. Metal producers have attempted to improve the SCC properties for HTH material by controlling trace element levels and modifying thermomechanical processing parameters. In this paper, the original and modified heats are referred to as original process heats and process variation heats, respectively.

The nature of SCC of Alloy X-750 in low and high temperature water is presented in this paper. It is shown that regardless of heat treatment, this material is susceptible to rapid cracking in low temperature water that is associated with a hydrogen-assisted cracking mechanism. The LTCP behavior was characterized by testing fracture mechanics specimens to establish the critical stress intensity factor (K_I) for rapid cracking as a function of test temperature, hydrogen content of the water, load history and heat treatment. The role of hydrogen was established by comparing the cracking behavior in low temperature water with that in hydrogen-precharged specimens tested in air. Auger electron spectroscopy (AES) of materials given various heat treatments was performed to relate grain boundary segregation to cracking susceptibility. To

characterize the HTSCC response, tests on fracture mechanics specimens were performed in 288° to 360°C water. The parameters studied included the time required to initiate SCC from a notch, time required to incubate SCC from a fatigue precrack, and crack growth rates.

EXPERIMENTAL PROCEDURE

Materials

Materials given the AH, BH and HTH heat treatments were included in this study. The chemical composition of the heats is provided in Table 2. The first letter of the heat identification represents the material supplier (from "A" to "E"). Heat numbers are consistent with those in Reference (7). Heats A2, A6 and A17 and A18 are process variation heats; all others are original process heats. Some of the heats were given two different heat treatments, as indicated in Table 2.

Typical microstructures are shown in Figure 1. The AH and BH materials exhibited a fine grain size (ASTM No. 8-10), whereas the HTH heats exhibited a coarse grain size (ASTM No. 2-4) as a result of the high temperature solution anneal. The room temperature tensile properties are summarized in Table 3. The yield and ultimate strength levels for both AH and HTH materials are significantly lower than those for BH materials, because the latter is direct aged after hot working.

Test Specimens

Tests were performed on compact tension (CT) specimens with a width of 20.3 mm and a thickness of 10.2 mm and three-point-bend specimens with a width of either 10 or 8.3 mm and a thickness of 5.6 mm. The root radii in specimens tested in the as-notched condition ranged from 0.1 to 0.76 mm and notches were finished by low stress grinding. Precracked specimens were prepared per ASTM E399 procedures with a maximum K_I of 20 MPa$\sqrt{m}$ during the final precrack interval. The nominal crack length or notch length to width ratio (a/W) was 0.5 for all tests.

Conventional CT specimens were used in rising load tests and constant-load SCC tests. For constant-displacement SCC tests, a threaded hole was machined along the load line in one of the specimen arms in order to bolt load the specimens.

Test Methods

Low temperature crack growth tests

The LTCP response was characterized by 1) rising load testing of CT and three-point-bend specimens, 2) constant-displacement testing of bolt-loaded CT specimens and 3) controlled-load testing of CT specimens. Rising load tests were performed on both hydrogen-precharged and non-precharged specimens in air and water. Most water tests were conducted at a constant displacement rate with a $\dot{K}$ of about 4 MPa$\sqrt{m}$/h based on the original precrack length. Prior to testing, specimens were preconditioned for two weeks in 288° to 360°C water with high hydrogen (30-60 cc H_2/kg H_2O). It is noted that non-precharged specimens tested in water and hydrogen-precharged specimens tested in air exhibited rapid low temperature cracking at $\dot{K}$ values as high as 100 MPa$\sqrt{m}$/h. Limited slow rate testing was performed at $\dot{K}$ values as low as 0.3 MPa$\sqrt{m}$/h to assure that there was sufficient time for fully developing hydrogen enrichment in the peak stress region ahead of a crack. A few hydrogen-precharged specimens were rapidly loaded at a $\dot{K}$ of about 3000 MPa$\sqrt{m}$/h to preclude hydrogen from diffusing and accumulating ahead of the crack. Stress intensity factor calculations were performed in accordance with ASTM E399 procedures.

The key parameters in rising load tests are the K_I value at maximum load (K_{Pmax}) and the time required to go from maximum load to one-half maximum load ($t_{1/2Pmax}$). Only K_{Pmax} values are reported herein. It is noted that at a $\dot{K}$ of 4 MPa$\sqrt{m}$/h, typical $t_{1/2Pmax}$ values are less than 1 minute for susceptible AH and BH heats and greater than 4 minutes for HTH heats. Once LTCP initiated in these tests, the rate of load drop was used to estimate crack growth rates in accordance with the Saxena-Hudak compliance relationship.[8]

In Alloy X-750 with yield strengths from 760 to 1030 MPa, linear-elastic fracture mechanics concepts are valid up to K_I levels of about 65 MPa$\sqrt{m}$. Higher K_{Pmax} values are reported for heats with high SCC resistance. While these values are not strictly valid, they provide a relative ranking of SCC susceptibility.

Constant-displacement testing of bolt-loaded CT specimens was conducted to determine the critical stress intensity factor ($K_{ISCC-LT}$) below which LTCP does not occur. Bolt loading was accomplished by a load transfer method, whereby specimens were pin loaded to 95% of the

desired load in a tensile machine and then the load was transferred to the bolt. This was done by torquing the bolt, followed by partially reducing the load in the load train, and then retorquing the bolt until the desired crack mouth opening displacement (CMOD) was obtained. This process was repeated until the machine load was completely removed. Bolt-loaded specimens were then tested in autoclaves at various temperatures and water hydrogen contents. Most bolt-loaded specimens were preconditioned in 288°to 360°C high hydrogen water for approximately two weeks and then slowly cooled through the critical temperature regime (150° to 24°C) to initiate LTCP. The value of $K_{ISCC\text{-}LT}$ is taken to be either the value of K_I where the intergranular crack arrests or the applied K_I level below which LTCP did not occur.

Cooldown testing of CT specimens under constant or slightly increasing load was also performed to compare $K_{ISCC\text{-}LT}$ obtained under these loading conditions with critical K_I values obtained in constant-displacement and rising load tests. The load was applied while specimens were exposed to 288°C high hydrogen water. During cooling to 24° or 54°C, the load was held constant or continuously increased. Some specimens were held for 12 to 21 days in 54°C water following the cooldown in an attempt to increase the opportunity for LTCP to occur. A few specimens were also tested under constant-load conditions directly at the test temperature without high temperature preconditioning.

High Temperature SCC Tests

High temperature SCC properties were characterized by testing precracked CT specimens under constant-load or constant-displacement conditions in 288° to 360°C high hydrogen water. The key parameters in these tests are the time to initiate SCC from a notch (t_{INI}), time to incubate SCC from a precrack (t_{INC}), and crack growth rate (da/dt). During constant-load tests, specimens were exposed to high temperature water prior to loading, and in-situ LVDT measurements of the crack mouth opening displacement (CMOD) were used to determine when crack incubation occurred. The bolt-loading method for constant-displacement tests was the same as described above. After bolt loading, specimens were exposed to 288° to 360°C water containing 40 to 60 cc H_2/kg H_2O. Whenever HTSCC tests were interrupted and cooled below 175°C, the water hydrogen content was reduced below 20 cc H_2/kg H_2O to minimize the potential for LTCP.

Periodically, specimens were removed from autoclaves to determine crack incubation times and crack growth rates. Surface crack length measurements were made visually on all specimens,

but significant crack tunneling is typical, so cracking in the center of the specimen is significantly greater than that observed on the surface. To account for tunneling, the average crack size was estimated based on residual load measurements made by using the load transfer method in reverse. Specifically, the bolt load was transferred to the tensile machine, while never unloading the crack tip by more than 2-3%. The crack length was then determined from the residual bolt load via the Saxena-Hudak compliance relationship.[8] Destructive evaluation of specimens was performed to confirm LVDT and residual bolt load results.

The majority of tests were conducted in water with a room temperature pH between 10.1 and 10.3, an oxygen content less than 100 ppb, and conductivity between 20 and 85 μS/cm. Some rising load tests were performed in 93°C argon-sparged deionized water at atmospheric pressure.

Hydrogen Precharging

Hydrogen precharging was accomplished by encapsulating specimens in an argon-purged chamber containing tantalum hydride which was then heated to 704°C for one to four hours. This temperature was chosen since it corresponds to the final aging temperature for all three heat treatments. Diffusional calculations show that the exposure time is sufficient to produce a uniform concentration of hydrogen in specimens. To minimize hydrogen loss after charging, specimens were refrigerated below 0°C up to the time of testing. Vacuum extraction analysis was performed after testing to determine hydrogen contents which typically ranged from 25 to 60 ppm.

Hydrogen Diffusion Measurements

Hydrogen diffusion in Alloy X-750 was characterized by hydrogen penetration and hydrogen desorption studies of three BH heats. Diffusion penetration data was obtained by hydrogen analysis of layers machined from a specimen that was cathodically charged at 85°C for 89.8 hours. The hydrogen concentration profile fit the following function:[9]

$$\frac{C}{C_s} = 1 - erf\left(\frac{x}{2\sqrt{Dt}}\right) \qquad (1)$$

where D is the diffusion coefficient, C is the hydrogen concentration at distance, x, and time, t, and C_s is the surface concentration, assumed to be constant.

Diffusion coefficients corresponding to hydrogen desorption at 24° and 316°C were made based on hydrogen analyses immediately after charging and again after long term storage at 24°C or after a short period of time at 316°C, where substantial desorption did occur. It was assumed that the surface offered no resistance. The geometry was assumed to be a semi-infinite plate with the actual thickness, for which solutions are provided in Reference (9). For the 316°C test where desorption is large, this is a reasonable assumption because hydrogen is lost predominantly through the large surface normal to the minimum (thickness) direction. However, at 24°C where desorption was relatively small and diffusional loss was confined to the near-surface region, a correction was introduced by simply reducing the observed desorption by 35%, which represents the ratio of the edge surface area (i.e., 2 x Width x Length) to the total surface area.

Auger Electron Spectroscopy

The grain boundary chemical composition was obtained by in-situ Auger analysis of intergranular surfaces. To assure intergranular fracture, small notched cantilever bend specimens suitable for fracture in the AES high vacuum chamber were hydrogen precharged by the procedures outlined above. After fracturing in a vacuum of less than 10^{-7} Pa, specimens were examined in the scanning electron microscope (SEM) mode to identify approximately ten intergranular facets for AES analysis.

RESULTS

Low Temperature Crack Propagation Results

The rising load test results in Figure 2 illustrate the profound influence of low temperature water on the cracking performance of a particularly susceptible BH heat. In 93°C air this heat exhibits good fracture resistance with a K_{Pmax} value of 128 MPa$\sqrt{m}$. While the actual toughness is even higher because maximum load is limited by plasticity effects, this K_{Pmax} value demonstrates that this material has superior fracture toughness. In 93°C argon-sparged water, however, environment-induced cracking severely degrades fracture resistance as K_{Pmax} is reduced to 45 MPa$\sqrt{m}$. This dramatic effect is associated with a fracture mechanism transition from ductile dimple rupture in air to intergranular LTCP in water. Cracking in low temperature water initiates well within the linear-elastic domain and the rapid crack advance leads to failure within 1 minute. For this BH heat, the Stage II crack growth rate was determined to be 7.2 mm/min at 93°C.

The effects of water temperature and hydrogen content on K_{Pmax} values from rising load tests are summarized in Figures 3 and 4. For comparison, K_{Pmax} values in air, ranging from 90 to 130 MPa$\sqrt{m}$, are represented by the arrows on Figure 3. As noted earlier, K_{Pmax} levels in this range are overly conservative due to plasticity effects and the actual K_{IC} fracture toughness is closer to 150 MPa$\sqrt{m}$.[10] For example, J_{IC} testing of a CT specimen (width = 30.5 mm) from HTH Heat A10 yielded a K_{Pmax} of 115 MPa$\sqrt{m}$ and an equivalent K_{JC} of 156 MPa$\sqrt{m}$.

For susceptible AH and BH heats, K_{Pmax} values are significantly reduced in water. AH heats exhibit a wide range of LTCP properties and the results in Figures 3a and 4 represent typical susceptible heats. BH heats tend to be more susceptible to LTCP and the data shown in Figure 3b are representative, although it is noted that some BH heats display good resistance to LTCP. HTH heats tend to have superior LTCP resistance and the typical behavior is represented in Figure 3c. While the degree of susceptibility for HTH heats is relatively small in water with 16 cc H_2/kg H_2O, the fracture resistance is decreased markedly in 24° to 94°C water with 60 cc H_2/kg H_2O. Two common heats were tested in both the BH and HTH conditions, and comparison of the solid symbols in Figures 3b and 3c shows the clear superiority of the HTH treatment.

Considerable scatter is common in rising load tests, so lower bound curves for K_{Pmax} are shown in Figure 3 for 16 and 35-60 cc H_2/kg H_2O to illustrate the overall behavior. In low hydrogen

water (10-20 cc H_2/kg H_2O), the minimum K_{Pmax} occurs (at a $\dot{K}$ of 4 MPa $\sqrt{m}$/h) between 55° and 120°C and there is a marked increase in K_{Pmax} at room temperature, regardless of heat treatment. In high hydrogen water, the minimum K_{Pmax} occurs at about 55°C and there is very little increase in toughness at room temperature.

Figure 4 shows that increasing the hydrogen content of the water decreases LTCP resistance, with the largest effect occurring below 25 cc H_2/kg H_2O. The greater susceptibility with increasing hydrogen overpressure is believed to be associated with greater hydrogen absorption due to an increase in the equilibrium concentration of nascent hydrogen and formation of less protective oxide films. Figure 4 also indicates that heats with a low toughness in 16 cc H_2/kg H_2O show the least reduction in K_{Pmax} with further increases in hydrogen content. This behavior suggests that a threshold K_I level exists below which higher hydrogen levels do not further degrade fracture toughness. Extrapolation of the trends indicate that the apparent threshold K_I is on the order of 30 MPa$\sqrt{m}$ for susceptible AH and BH heats and 40 MPa$\sqrt{m}$ for HTH heats. In argon-sparged deionized water, the majority of heats show a dramatic improvement in LTCP resistance, which is expected as the water hydrogen content is reduced to zero. Three heats showed little change in K_{Pmax} between 0 to 16 cc H_2/kg H_2O (represented by dotted lines in Figure 4), but this behavior is attributed to data scatter as each of these heats exhibit unusually large decreases in K_{Pmax} between 16 and 25 cc H_2/kg H_2O.

While the rising load test results presented above are directly applicable under increasing load conditions, testing has shown that these results also provide lower-bound threshold stress intensity factors ($K_{ISCC\text{-}LT}$) for constant-displacement and constant-load conditions, as described below. Under strictly constant-load conditions during cooling, no LTCP occurred for a series of K_I levels well above those that produced cracking in isothermal rising load tests. As shown in Figure 5, no cracking occurred in AH and BH specimens that were cooled from 288°C under constant-load conditions in high hydrogen water, even though applied K_I levels were well above K_{Pmax} values from rising load tests (denoted by solid lines). The AH specimen was subjected to three coolings at successively higher K_I levels of 38, 47 and 57 MPa$\sqrt{m}$. No evidence of LTCP was observed even after a 21 day hold in 54°C high hydrogen water at the highest K_I level. Following constant-load testing, this specimen yielded a rising load K_{Pmax} value of 38 MPa$\sqrt{m}$, which was just slightly higher than that obtained in previous rising load tests on this heat, represented by the solid line. Similar behavior was observed for a BH heat with K_{Pmax} values ranging from 28 to 49 MPa$\sqrt{m}$ at 54° to 150°C. Two successive coolings under constant-load

conditions with a K_I of 49 MPa$\sqrt{m}$ failed to produce LTCP, even after a 12 day hold in 54°C water, the most susceptible temperature. Subsequent rising load testing of this BH specimen yielded a K_{Pmax} of 34 MPa$\sqrt{m}$, which was only slightly higher than the previously determined K_{Pmax} value for this heat at 54°C. The modest increase in K_{Pmax} after constant-load testing was attributed to an overload or prestrain effect that retarded subsequent cracking. Constant-load cooldown tests were not conducted on HTH specimens.

Results from cooldown testing of two BH heats and one HTH heat under mildly increasing loads (by ~10%) are shown in Figure 6. In these tests, the increase in load represents the load change observed under constant-displacement conditions during continuous cooling due to an increase in elastic modulus. LTCP is seen to occur under temperature and K_I conditions that are consistent with rising load K_{Pmax} results, designated by the solid lines. Thus, K_{Pmax} represents the critical stress intensity factor ($K_{ISCC\text{-}LT}$) for LTCP under mildly or significantly increasing loads.

Figure 7 compares rising load K_{Pmax} values with critical LTCP stress intensities based on constant-load and constant-displacement tests where specimens were exposed to low temperature water for times up to one year. The data from Figure 6 obtained under mildly increasing load conditions are also included in this plot. When K_I values were higher than K_{Pmax}, LTCP occurred in periods as short as 2 days and as long as 60 days. Therefore, if the applied K_I is greater than $K_{ISCC\text{-}LT}$ cracking may occur at any time. Comparison of constant-load results in Figures 5 and 7 indicates that high temperature exposure of precracked specimens has a mitigating effect on cracking in low temperature water. Specifically, LTCP did not occur in constant-load tests after continuous cooling from 288°C (Figure 5), but did occur in constant-load specimens that were exposed only to low temperature water (Figure 7). The reason for increased fracture resistance after high temperature exposure is not clear but may be associated with development of a protective oxide film in high temperature water. Auger analysis revealed that the primary difference in oxide films formed in low and high temperature water is their thickness. Films formed in 54°C water had a thickness of about 50 Å, whereas 288°C films were an order of magnitude thicker. It is possible that a thick film serves as a diffusion barrier or promotes more effective recombination of hydrogen. Because less nascent hydrogen is available to enter the metal, specimens with a thick high-temperature oxide film resist LTCP. Crack tip strains associated with rising load conditions or continuous cooldowns under increasing load conditions rupture the thick protective oxide which enhances hydrogen pickup.

It is significant that survivors as well as failures are possible when K_I is greater than $K_{ISCC\text{-}LT}$. When bolt-loaded CT specimens tested in water with 35 to 60 cc H_2/kg H_2O were repeatedly cooled from 246° - 360°C to room temperature, the number of cooling cycles prior to sudden massive low temperature crack extension ranged from 1 to 21 at K_I levels approximately twice K_{Pmax}. Thus, survival for some period above $K_{ISCC\text{-}LT}$ is possible, but sudden failure may occur at any time.

The degree of conservatism in rising load tests appears to be dependent on material susceptibility. Figure 7 shows that rising load K_{Pmax} values conservatively predict $K_{ISCC\text{-}LT}$ for materials with high and intermediate susceptibility (K_{Pmax} < 45 MPa$\sqrt{m}$). For more resistant materials such as process variation HTH heats, rising load K_{Pmax} values provide a reasonable estimate of $K_{ISCC\text{-}LT}$, but are not always conservative. Apparently, the conventional rising load strain rate of $\dot{K} \approx 4$ MPa$\sqrt{m}$/h is too fast to allow for sufficient hydrogen accumulation to fully embrittle grain boundaries in resistant materials. This is supported by the observation of lower K_{Pmax} values with an order of magnitude decrease in strain rate.

In summary, the conventional rising load test is an appropriate and effective method for conservatively predicting the critical K_I for LTCP in susceptible heats, while it provides a reasonable, but not necessarily conservative, estimate of the critical K_I for SCC resistant heats. Although a lower strain rate test provides a lower K_{Pmax} value, the long test time generally prohibits its use for production testing. To obtain a conservative $K_{ISCC\text{-}LT}$ value for highly resistant materials, crack arrest testing of multiple bolt-loaded CT specimens under continuous cooldown conditions is recommended.

Low temperature cracking of AH and BH materials involves a classic two-stage behavior, with growth rates being independent of K_I over a wide range of stress intensities (Stage II). Figure 8 shows that Stage II crack growth rates fit an Arrhenius law [$da/dt = A \exp(-Q_{LTCP}/RT)$] with an activation energy, Q_{LTCP}, of 11.3 kcal/mol. Crack growth rates for this BH heat tested in 32°-54°C argon-sparged water are on the order of 0.02 to 0.2 mm/hour. Stage II LTCP rates for susceptible heats in 93°C water can be as high as 400 mm/hour.

Low Temperature Crack Propagation Mechanism

The nature of the LTCP phenomenon was characterized by testing hydrogen-precharged specimens under various conditions. The findings demonstrate that cracking in low temperature water is controlled by a hydrogen embrittlement mechanism where hydrogen is generated by corrosion reactions at the crack tip. Key findings from this study are summarized below:

1. Precharged specimens tested in air demonstrated that hydrogen alone, without corrosion, produced intergranular fractures indistinguishable in fractographic appearance from those produced in low temperature water (Figure 9). Non-precharged specimens tested in air typically fail in a transgranular manner.

2. Stage II crack growth rates in low temperature water are controlled by hydrogen diffusion from the water-metal interface to the maximum hydrostatic stress region ahead of the crack tip. This conclusion is based on the equivalency of activation energies for crack growth rate (11.3 kcal/mol) and hydrogen diffusion (11.5 kcal/mol). The activation energy for hydrogen diffusion was based on hydrogen desorption measurements at 24° and 316°C and hydrogen penetration measurements for a cathodically-precharged specimen at 85°C. As shown in Figure 10, the activation energy of 11.5 kcal/mol was in excellent agreement with the 11.7 kcal/mol reported for Alloy X-750[11] at 204° to 315°C and the 11.9 kcal/mol reported for nickel-base superalloy Alloy 718[12] over a wide range of temperatures. In addition, the room temperature diffusivity, 3.0×10^{-11} cm^2/s, agreed reasonably well with the value of 5.6×10^{-11} cm^2/s determined for Alloy X-750 by Latanision and Kurkela[13].

3. Figure 11 shows that the fracture toughness of hydrogen-precharged AH and BH specimens tested in air is comparable to their non-precharged counterparts tested in low temperature water with 16 cc H_2/kg H_2O. While the toughness of hydrogen-precharged HTH specimens is substantially lower than K_{Pmax} for non-precharged specimens tested in water with 16 cc H_2/kg H_2O, it is only slightly lower than the K_{Pmax} value of ~40 MPa$\sqrt{m}$ obtained in water with 60 cc H_2/kg H_2O (see data for HTH Heat B5 in Figure 3). Comparison of the air and water data for BH and HTH Heat B5 (Figures 11b and 11c) clearly demonstrates that the superior performance of the latter in water with 16 cc H_2/kg H_2O is due to increased resistance to hydrogen pickup from the corrosion reaction,

because both materials are equally susceptible to hydrogen embrittlement when precharged to 62 ppm hydrogen. The difference in hydrogen absorption for BH and HTH materials is believed to be influenced by grain boundary species such as phosphorus and sulfur, as discussed later. In the high hydrogen water, hydrogen absorption in the HTH material is enhanced due to the increased concentration of nascent hydrogen.

4. The most severe hydrogen embrittlement occurred when precharged specimens were tested in low temperature water. In this case, hydrogen produced by the corrosion reaction combined with hydrogen already present to severely weaken grain boundaries as well as fill traps and interact with dislocations. This indicates that the corrosion reaction in water further increased the local hydrogen content within the high triaxial stress region ahead of crack.

The magnitude of hydrogen enrichment and how it relates to the concept of critical hydrogen concentration for intergranular cracking was assessed by relating hydrogen-precharged specimen results to the LTCP phenomenon in water. Testing of hydrogen-precharged specimens was performed at both high and low strain rates to determine the critical hydrogen concentration for intergranular cracking and how hydrogen concentrates in the hydrostatic stress field ahead of the crack tip. Data from variable strain rate tests were used to select the slow and fast loading conditions where K_{Pmax} values were independent of displacement rate (i.e., either sufficient time to develop full embrittlement in slow tests or insufficient time to permit hydrogen diffusion in fast tests). At 93°C, a $\dot{K}$ of 600 MPa$\sqrt{m}$/h was sufficiently slow for hydrogen enrichment to develop in the peak stress region ahead of the crack, while a five-fold increase in $\dot{K}$ prevented significant hydrogen concentration. At 24°C where diffusion rates are about fifty times slower, a $\dot{K}$ of 600 MPa$\sqrt{m}$/h was fast enough to preclude hydrogen enrichment. To assure sufficient time for concentrating hydrogen ahead of the crack tip, slow rate testing at room temperature was performed at 0.3 MPa$\sqrt{m}$/h. Intergranular cracking was observed in all precharged specimens tested at slow strain rates and in specimens with high hydrogen concentrations tested at high strain rates, as detailed below.

In high rate tests of precharged specimens, the local concentration was taken to be the bulk hydrogen content because there was insufficient time to allow hydrogen to diffuse and accumulate ahead of the crack. These fast tests showed that the critical bulk hydrogen concentration required to induce intergranular fracture was about 25 ppm and the corresponding

K_{Pmax} value was 55-60 MPa$\sqrt{m}$. When the concentration increased to about 50-100 ppm, K_{Pmax} decreased to 40-50 MPa$\sqrt{m}$, which is consistent with K_{Pmax} values associated with rapid intergranular cracking in low temperature water. Hence, the critical hydrogen concentration required to produce LTCP in water is about 50-100 ppm.

In slow rate tests, there is sufficient times for hydrogen to diffuse to the triaxial stress region ahead of the crack. The local concentration under chemical equilibrium conditions was calculated by the relationship[14]

$$\frac{C}{C_O} = \exp \frac{\sigma_H \bar{V}}{RT} \qquad (2)$$

where C and C_o are the local and bulk concentrations, σ_H is the hydrostatic stress, $\bar{V}$ is the partial molar volume of hydrogen in solid solution, R is the universal gas constant and T is absolute temperature. $\bar{V}$ is defined as the change in volume produced by the addition of 1 gram-mol of hydrogen into the metal. The value for Alloy X-750 was estimated to be 1.8 cm^3/mol based on lattice parameter measurements for solutions of hydrogen in nickel and other face-centered cubic metals[15, 16]. This value represents the lower bound of values reported for hydrogen in iron and steel.[17] Rice[18] showed that the maximum normal stress, σ_{yy}, inside the plastic zone is essentially independent of K_I. The effect of increasing K_I is to expand the peak stress over a wider region and locate the peak stress region farther from the crack tip. The magnitude of the peak stress, σ_{yy}, is about $3.5\sigma_{YS}$ for a strain-hardening material such as Alloy X-750. Assuming plane strain conditions, the peak hydrostatic stress is about 50% to 60% of the peak normal stress or twice the yield strength, which is within 5% of the peak hydrostatic stress assumed by Gerberich et al.[19] This relationship was incorporated into Eq. (2) to estimate the maximum C/C_o ratios as functions of temperature and yield strength (see Figure 12). It is seen that peak C/C_o ratios range from 1.7 at 360°C to 3.2 at 24°C for a yield strength of 800 MPa (representative of Conditions AH and HTH) and from 1.9 at 360°C to 4.2 at 24°C for a yield strength of 1000 MPa (representative of Condition BH).

The K_{Pmax} values for fast and slow rising load tests of hydrogen-precharged specimens conducted in 24° and 93°C air are shown in Figure 13. As expected, there is no correlation between K_{Pmax} values and bulk hydrogen content. However, the calculated local hydrogen enrichment for the slow tests, based on the peak C/C_o ratios given in Figure 12, and measured bulk content for fast

tests provide a reasonable correlation with K_{Pmax}, as represented by the solid line in Figure 13. Thus, the stress intensity factor causing intergranular cracking in hydrogen-precharged specimens is correlated with the local hydrogen content ahead of the crack tip. By assuming this correlation holds regardless of the source of hydrogen, the observed K_{Pmax} values for LTCP in water suggest that about 100 ppm hydrogen is absorbed due to the corrosion reaction and concentrated ahead of the crack as a result of diffusion to the high triaxial stress region.

Temperature effects on K_{Pmax} for hydrogen-precharged material are shown in Figure 14. These tests were performed at relatively high rates (0.05 mm/min at 93°C, 0.05 mm/min for AH and 0.13 mm/min for HTH at 149° and 204°C, and 0.51 mm/min at 288°C) so hydrogen content would not decrease significantly during high temperature exposure. The beneficial effect of increasing temperature is apparent, with the degree of embrittlement and amount of intergranular cracking decreasing markedly above 150°C. The increased fracture resistance and evidence of some transgranular cracking above 150°C accounts for the absence of a rapid cracking mechanism in this temperature regime. The transgranular fracture surface observed in high temperature tests has a faceted, crystallographic appearance (Figure 15), indicative of channel fracture. This mechanism occurs when localized cracks initiate and propagate along intense dislocation channels, so the presence of a channel fracture mechanism indicates that hydrogen tends to promote planar slip.

In summary, accumulation of hydrogen ahead of the crack tip appears to be the critical factor for LTCP in water. The degree of embrittlement increases exponentially with peak hydrostatic stress, yield strength and notch acuity, as discussed below. Under the most severe conditions the maximum enrichment ratio is 3 to 4. Since this enrichment phenonemon diminishes with temperature, it is expected to have less importance for HTSCC.

Low Temperature Crack Propagation at Notches

As-notched specimens subjected to constant-displacement conditions have exhibited no evidence of cracking in low temperature water. The immunity to LTCP is attributed to the greater diffusion distance and less severe stress state for as-notched specimens, in comparison to those for precracked specimens (see Figure 16). The proximity of the peak stress position relative to the crack tip is particularly important. For notched configurations, the distance between the metal-water interface and peak stress location is relatively large, so hydrogen has to diffuse over

a considerable distance to reach the assumed crack nucleation site, as illustrated in Figure 16. Because the diffusion distance for as-notched specimens is about five times greater than that for precracked specimens, only a small fraction of the corrosion-generated hydrogen reaches the critical peak hydrostatic location ahead of a notch due to diffusion loss in the surrounding matrix.

During rising load testing of as-notched specimens in low temperature water, ductile tears form near maximum load as a result of a microvoid coalescence mechanism, rather than intergranular cracking. The lack of intergranular cracking during the initiation stage is due to relatively low hydrogen enrichment resulting from the low peak hydrostatic stress and the large distance from the metal-water interface to the peak stress position. Once a ductile tear initiates at the notch root, additional crack extension occurs by an intergranular mechanism, as shown in Figure 17. In this case, the crack-like tear enhances hydrogen enrichment by increasing the peak hydrostatic stress and decreasing the distance from the crack tip to the peak stress position to about 0.03 mm, which minimizes diffusional losses.

When as-notched specimens are embrittled by hydrogen precharging, they are susceptible to intergranular crack initiation. Apparently, bulk hydrogen levels in precharged specimens produced sufficient hydrogen enrichment ahead of the notch to initiate intergranular cracking. This finding demonstrates that hydrogen enrichment, rather than peak stress conditions, control initiation of intergranular cracking ahead of a notch. Thus, the lack of intergranular crack initiation in non-precharged specimens tested in water must be due to diffusional loss over the large distance from the metal-water interface and the peak stress location. This is further supported by the as-notched specimen data (squares) in Figure 11a. While as-notched specimens are embrittled by hydrogen precharging, both precharged and nonprecharged specimens are essentially unaffected by the presence of water. This observation indicates that relatively little of the hydrogen picked up in low temperature water reaches the critical peak stress location due to diffusional loss in the surrounding matrix.

Effect of Grain Boundary Segregation on LTCP

AES studies of intergranular fracture surfaces were performed to characterize the grain boundary composition and relate it to LTCP properties. Figure 18 shows that LTCP resistance correlates with grain boundary phosphorus concentrations, but not bulk phosphorus levels. An increase of intergranular phosphorus content from 1 to 4 atomic percent results in a 60% decrease in K_{Pmax},

from 110 to 45 MPa$\sqrt{m}$. As a hydrogen recombination poison, phosphorus promotes hydrogen absorption by retarding recombination of corrosion-generated nascent hydrogen into molecular hydrogen, which cannot be absorbed into the metal. In addition, phosphorus reduces grain boundary cohesive strength during the hydrogen-assisted cracking process. Interactions of hydrogen and phosphorus may also be involved in high temperature SCC, but definitive information is lacking.

Comparison of results in Figure 18 also demonstrates that the degree of segregation varies widely in BH heats, is very high in the AH heat, and is generally low in HTH heats. The nature of phosphorus segregation to grain boundaries was investigated by AES to understand the role of heat treatment. Increasing the annealing temperature from 954° to 1121°C was found to cause a continuous decrease in intergranular phosphorus concentration, whether or not grain coarsening occurred. Specifically, grain boundary phosphorus contents for two BH heats decreased from 2.6-2.7 atomic percent in the as-received condition to 0.2-0.6 atomic percent after the 1121°C anneal. The high temperature anneal also caused considerable grain growth that had a profound effect on segregation kinetics during subsequent re-aging at 704°C, as shown in Figure 19. Coarse grained specimens annealed at 1121°C exhibited a segregation rate during 704°C aging that was almost two orders of magnitude less than that for specimens annealed at 954°C, which did not show grain coarsening. Grain coarsening *per se* does not retard segregation; in fact, it often has the opposite effect as coarse grain structures have less boundary area so greater concentrations can be achieved. For Alloy X-750, however, grain boundary migration alters the nature of the boundaries which retards segregation during subsequent thermal aging. It is postulated that the retarded phosphorus segregation in coarse grained material aged at 704°C is associated with a chemical interaction of phosphorus with niobium and titanium. These species have been shown to react with phosphorus to reduce grain boundary segregation in iron and steels[20, 21]. In fine grained AH and BH materials, small niobium and titanium-rich MC-type carbides decorate grain boundaries (as discrete particles or thin films) and thereby reduce the amount of niobium and titanium available to tie up phosphorus. The high temperature HTH anneal dissolves these carbides or keeps them from forming and results in the formation of intergranular chromium-rich $M_{23}C_6$ carbides. The increased concentration of niobium and titanium then reduces the effective matrix concentration of phosphorus which has a strong effect on segregation kinetics. Alternatively, the niobium and titanium-rich MC type interfaces present in Condition AH and BH materials may simply be more susceptible to phosphorus segregation than the $M_{23}C_6$ interfaces in Condition HTH material.

AES studies also showed that an intermediate age at 954°C after the 1121°C anneal enhances subsequent segregation at 704°C, as shown in the following comparison:

Treatment	Grain Boundary P (at. %)
BH + 704°C-1 h	2.7
BH + 1121°C-1 h + 704°C-1 h	0.58
BH + 1121°C-1 h + 954°C-1 h + 704°C-1 h	1.2
BH + 1121°C-1 h + 704°C-20 h	0.67
BH + 1121°C-1 h + 954°C-1 h + 704°C-20 h	1.5

(Note that all specimens were hydrogen precharged at 704°C for at least one hour to induce intergranular fracture.) It is seen that the 1121°C anneal caused a factor of five reduction in phosphorus concentration, relative to the starting BH material. While direct aging at 704°C for times up to 20 hours caused relatively little phosphorus segregation, duplex aging at 954° and 704°C doubled phosphorus segregation. Some of this increase was caused by segregation at 954°C, but a significant amount occurred at 704°C due to an enhancing effect of the intermediate temperature. The 954°C treatment is likely to immobilize some of the niobium and titanium by carbide precipitation, thereby increasing the effective matrix concentration of phosphorus at 704°C.

Thus, the 885°C stress equalization and 704°C age in the AH treatment results in significant phosphorus segregation and poor LTCP properties, even in heats with low bulk contents. BH materials tend to exhibit poor LTCP properties due to significant phosphorus segregation resulting from direct aging of the fine grained material at 704°C in addition to its higher strength which enhances hydrogen concentration in the peak stress region ahead of the crack. The good LTCP resistance of Condition HTH is associated with minimizing phosphorus segregation by altering the grain boundary structure during high temperature annealing and the avoidance of reheating at intermediate temperatures above 704°C.

While grain boundary phosphorus content was correlated with heat-to-heat variability in LTCP performance for Conditions AH and BH and the overall improvement in behavior for HTH materials, it appears to have only a weak correlation with heat-to-heat variability of the latter, as HTH heats typically have less than 2 atomic percent grain boundary phosphorus levels . To establish the cause of heat-to-heat variability for HTH heats, rising load testing and AES analyses were performed on one original process HTH heat and four process variation HTH heats. One

BH heat was also included in this study for comparison with earlier results. Figure 20 shows that K_{Pmax} values for HTH heats are not correlated with grain boundary phosphorus because the coarse grain structure consistently produces low grain boundary concentrations (1.1 to 1.7 atomic percent). The BH heat with more than double the grain boundary phosphorus (3.6 atomic percent) exhibited a low K_{Pmax} value of 46 MPa$\sqrt{m}$, which is consistent with the trend in Figure 18. Figure 20 does, however, implicate grain boundary sulfur as being detrimental to SCC performance in HTH heats. This is not surprising because sulfur is also a hydrogen recombination poison, just like phosphorus, and it is known to reduce grain boundary cohesive strength in nickel alloys. Thus, it is expected to play a role in hydrogen absorption and embrittlement. Unlike phosphorus, which showed no correlation between grain boundary and bulk concentrations, the decrease in grain boundary sulfur in process variation HTH heats is associated with reduced bulk content, which is shown parenthetically in Figure 20. Grain boundary sulfur may have played a role in the SCC performance of AH and BH heats, but preliminary AES studies indicated that local sulfur levels were generally much lower (<0.3 atomic percent) than phosphorus levels. As a result, grain boundary analysis of sulfur was not performed for the materials represented in Figure 18.

High Temperature Stress Corrosion Crack Initiation

High temperature SCC tests were performed in 288° to 360°C water with high hydrogen to determine the time required to initiate an intergranular stress corrosion crack from a notch, the time required to incubate a stress corrosion crack from a pre-existing fatigue crack, and SCC rates. Crack initiation times in 360°C water were obtained by testing as-notched CT specimens with various root radii and results are plotted as a function of peak surface elastic stress (PSES) in Figure 21. PSES is defined as the product of the theoretical stress concentration factor (K_t) and nominal stress (σ). Maximum stress levels at the notch roots are well beyond the yield strength, so PSES is more a measure of surface strain than the actual stress. It is seen that data for the AH material[1] are reasonably well fitted to a power law with an exponent (n) of -0.8, indicating that PSES is effective in normalizing data for various root radii (ρ). The PSES parameter is related to the $K/\sqrt{\rho}$ parameter used to correlate fatigue crack initiation data for

[1]About half of the AH specimens represented in Figure 21 were prestrained (i.e., intentional application of an initial load that is higher than the final load) either 5% or 10%. These prestrain levels had no effect on SCC performance. Use of 0%, 5% and 10% prestrain data, therefore, provides a better evaluation than reliance on the 0% group alone.

notched specimens. Based on the work of Creager and Paris,[22] Wilson [23] and Glinka,[24] the stress field ahead of a notch tip can be given in terms of the stress intensity factor K, which is equal to the following:

$$K = \frac{K_t \sigma \sqrt{\pi \rho}}{2} \tag{3a}$$

Rearranging terms and substituting PSES for ($K_t \sigma$), it is seen that PSES is proportional to $K/\sqrt{\rho}$:

$$PSES = \frac{2K}{\sqrt{\pi \rho}} \tag{3b}$$

Hence, the correlation given in terms of PSES could also be given in terms of $K/\sqrt{\rho}$.

SCC initiation times for Condition HTH, represented by the solid symbols in Figure 21, are two to three orders of magnitude greater than their AH counterparts. After 273 weeks of exposure in 360°C water, three of six specimens with PSES values between 2030 and 3050 MPa showed no SCC. At higher PSES values, all specimens showed SCC with initiation times ranging from 35 to 237 weeks. This contrasts with the poor AH performance where all of the specimens loaded to PSES values as low as 1060 MPa cracked prior to 3 weeks of exposure.

Typical of initiation behavior in an SCC resistant material, the observed times vary significantly under the same nominal conditions. A maximum likelihood analysis of the data for Condition HTH specimens revealed a power-law correlation between initiation time and PSES with an exponent of -1.4. This is approximately 50% higher than the stress exponent for Condition AH, suggesting that the improvement in SCC initiation times resulting from the HTH treatment is probably greater at low stresses.

<u>High Temperature Stress Corrosion Crack Incubation</u>

Precracked CT specimens were tested in 288° to 360°C water under both constant-displacement and constant-load conditions to characterize the time required to incubate intergranular cracking. The effect of applied K_I on the crack incubation time for Condition HTH in 360°C water is shown in Figure 22. Crack incubation times are based on residual bolt-load measurements for constant-displacement tests and in-situ LVDT measurements of the CMOD for constant-load tests. The amount of crack extension associated with crack incubation was 0.05

to 0.08 mm. High temperature SCC starts in less than 100 hours at K_I levels above 60 MPa$\sqrt{m}$ and after about 1000 hours at K_I levels of ~30 MPa$\sqrt{m}$. The incubation data for five HTH heats show very similar behavior, despite the different loading methods that were used. That is, the constant-load data from two heats and constant-displacement data from three different heats appear to fit a common curve. Crack incubation times are correlated by a power-law expressed by

$$t_{INC} = 1.7 \times 10^9 \, K_I^{-4.1} \tag{4}$$

where K_I is the stress itensity factor at 360°C in MPa$\sqrt{m}$ and t is in hours.

The effects of temperature on crack incubation times for constant-loaded AH and HTH specimens are shown in Figure 23. The incubation times fit an Arrhenius relationship with an activation energy, Q_{INC}, of 62 kcal/mol for Condition AH and 66 kcal/mol for Condition HTH. Incubation times for HTH materials are typically two to three orders of magnitude greater than those for AH materials under comparable test conditions. In Figure 23, the apparent difference is only a factor of five, but the HTH specimens were tested at a substantially higher K_I level. Taking the K_I dependency of Equation (4) into account in analyzing the data in Figure 23 indicates that the data support a 30-fold difference in crack incubation times for AH versus HTH materials.

High Temperature Stress Corrosion Crack Growth Rates

Crack growth rates obtained for bolt-loaded AH and HTH specimens are shown in Figures 24 and 25, respectively. Condition AH heats exhibit a classic two-stage crack velocity relationship with rates being independent of K_I between 20 to 45 MPa$\sqrt{m}$. Stage II rates, plotted in Figure 24, show an Arrhenius relationship with an activation energy, Q_{SCC}, of 33.7 kcal/mol. Crack growth rates for two HTH heats, shown in Figure 25, are dependent on both K_I and temperature. An Arrhenius fit with a power-law relationship with K_I provided an adequate description of the data:

$$\frac{da}{dt} = 1.1 \times 10^8 \, K_I^{4.3} \, e^{-Q_{SCC}/RT} \tag{5}$$

where da/dt is in μm/day, K_I is in MPa$\sqrt{m}$, T is in K, R is 1.987 cal K^{-1} mol^{-1} and Q_{SCC} is 41,400 cal/mol. It is seen that HTSCC rates for Condition HTH increased significantly with K_I, with a stress exponent (n) of 4.3, in contrast with the K_I independent response shown by Condition AH.

In addition, crack growth rates for Condition AH were 10 times faster than for Condition HTH at a K_I of 45 MPa$\sqrt{m}$ and almost 100 times faster at a K_I of 30 MPa$\sqrt{m}$.

The activation energy levels of 33.7 and 41 kcal/mol for HTSCC in water are slightly higher than those reported by Shen and Shewmon[25] for Alloy X-750 given a modified AH treatment[2] and tested in 300° to 400°C steam with high hydrogen. They found that Q_{scc} was dependent on applied K_I level (21, 28 and 51 kcal/mol at 61, 32 and 15 MPa$\sqrt{m}$, respectively). In the present study, Q_{scc} was independent of K_I level over the range tested (20 to 45 MPa$\sqrt{m}$ for Condition AH and 30 to 45 MPa$\sqrt{m}$ for Condition HTH).

Regardless of heat treatment, high temperature crack growth rates were much lower than LTCP rates. Even at 360°C, HTSCC rates were at least an order of magnitude lower than those observed at 54°C, indicating that the crack growth mechanisms in the two temperature regimes are very different. In fact, the high apparent activation energy levels for HTSCC clearly demonstrates that hydrogen diffusion is not the rate controlling process. Although hydrogen-assisted cracking is believed to be active in HTSCC, it is suspected that the controlling mechanism involves a thermally activated slip process. Support for a hydrogen-assisted cracking mechanism is the observation that the intergranular fracture surface morphology associated with HTSCC is indistinguishable from that observed in hydrogen-precharged specimens tested in air, as shown in Figure 26.

[2]Solution annealed at 982°C for 1 hour and air cooled. Aged at 816°C for 20 hours and air cooled. Aged at 704°C for 24 hours and air cooled.

DISCUSSION

Alloy X-750 exhibits an elastic-plastic fracture response with high J_{IC} values on the order of 100 kJ/m^2,[10] corresponding to an equivalent K_{IC} toughness of 150 MPa$\sqrt{m}$. In low temperature water, however, susceptibility to rapid cracking at K_I levels as low as 30 to 40 MPa$\sqrt{m}$ negates its inherent high fracture resistance. With LTCP rates as high as 7 mm/min, unstable fracture occurs very quickly once LTCP initiates, so applied stress intensities must be maintained below $K_{ISCC\text{-}LT}$ to preclude fast fracture.

The fast cracking results from embrittlement of grain boundaries by hydrogen that is generated by the corrosion reaction between low temperature water and the metal at the crack tip. Observed K_{Pmax} values in water indicate that critical hydrogen concentrations in the vicinity of a crack are on the order of 100 ppm. The peak triaxial stress state ahead of the crack makes an important contribution to the cracking mechanism since it acts on the hydrogen entering the metal due to the corrosion reaction. In the low temperature regime, triaxial stresses produce a three- to four-fold enrichment of hydrogen. The degree of enrichment diminishes markedly with temperature, so triaxial stress effects are expected to be less important at high temperatures.

Susceptibility to LTCP depends on temperature, hydrogen content of the water, heat treatment, susceptibility of a specific heat, loading rate and whether a crack is present. Low temperature cracking occurs below 150°C, but the temperature of maximum susceptibility, corresponding to a minimum $K_{ISCC\text{-}LT}$, occurs at 55°C for water with 35-60 cc H_2/kg H_2O and between 55° and 120°C in low hydrogen (<20 cc H_2/kg H_2O) water. This type of behavior indicates that competing processes are operative. The primary competing processes are believed to be generation of nascent hydrogen from the corrosion reaction, which can be absorbed into the metal, and its recombination into molecular hydrogen, which cannot be absorbed. With increasing temperature, more hydrogen is generated due to increased corrosion rates[26], but recombination reactions are also enhanced, resulting in reduced entry into the crack tip region. Higher temperatures also reduce the degree of hydrogen enrichment in the high triaxial stress region ahead of the crack. Under maximum susceptibility conditions, the combined effects of hydrogen generation, recombination and enrichment are optimized.

Hydrogen dissolved in the water increases hydrogen pickup by the metal and reduces $K_{ISCC\text{-}LT}$. Increasing the hydrogen content in the water increases the equilibrium atomic hydrogen at the

water-metal interface and may promote formation of less protective oxide films. Increasing the hydrogen content of the water from 15 to 35-60 cc H_2/kg H_2O typically decreases K_{Pmax} values by 25 to 50 percent. Thus, the hydrogen content should be reduced any time the water temperature is below 150°C to guard against LTCP. This was a real concern in the current tests when bolt-loaded specimens exposed at elevated temperatures were cooled to room temperature. To minimize the potential for LTCP, hydrogen levels in autoclaves were maintained below 20 cc H_2/kg H_2O whenever the temperature dropped below 175°C. For highly susceptible heats, K_{Pmax} values are not as sensitive to hydrogen content of the water between 15 and 60 cc H_2/kg H_2O, so the benefits of reduced hydrogen are not as great.

Susceptibility to LTCP varies widely for the different heat treatments and from heat-to-heat. This variability is generally associated with the degree of phosphorus and sulfur segregation to grain boundaries during material processing and heat treatment. Condition BH material is typically the most susceptible to LTCP due to its higher strength and phosphorus segregation to grain boundaries. The high yield strength increases crack-tip triaxial stresses that cause an exponential increase in hydrogen enrichment as well as an increase in the local stresses that serve as the crack driving force. In addition, 704°C aging of the fine grained structure results in significant phosphorus segregation that further degrades LTCP resistance. For Condition AH materials, the 885°C stress equalization preconditions grain boundaries which further increases phosphorus segregation during aging at 704°C, resulting in high concentrations, even in heats with relatively low bulk contents. The grain coarsening caused by the high temperature HTH anneal dramatically decreases the tendency for phosphorus segregation during subsequent 704°C aging, and this greatly improves SCC resistance. In Condition HTH material intergranular chromium-rich $M_{23}C_6$ carbides form, rather than niobium and titanium-rich MC carbides. As a result, the increased niobium and titanium in solution is believed to reduce the effective phosphorus concentration in the matrix and thereby reduce the degree of segregation. In HTH materials, reduced grain boundary sulfur was found to improve SCC performance. Since the decrease in grain boundary sulfur is associated with reduced bulk content, optimum melting techniques for improving ingot microcleanliness should be employed to provide maximum SCC resistance.

During cooling from high temperatures, the propensity for LTCP is highly sensitive to loading rate, with static loading conditions resulting in much greater resistance than rising load conditions. This sensitivity is significant because loads in many fastener applications increase during cooldown due to one or more sources. In joints comprised of materials with a similar thermal

expansion coefficient, the load increases during cooling due to an increase in elastic modulus. This produces a 10-15 percent increase in load during cooling from 288-360°C to 24°C. As shown in Figure 6, this rate of load increase is sufficient to produce LTCP at critical stress intensities equivalent to K_{Pmax} values obtained in rising load tests. If thermal expansion coefficients for the fastener and compression path are substantially different, significant uploading or unloading can occur during cooldown. In cases where the load increases markedly due to both modulus changes and differential thermal expansion, isothermal rising load results are directly applicable. When cooling results in no load change or a partial unloading, K_{Pmax} values conservatively predict cracking because LTCP is expected to be retarded. Since K_{Pmax} values accurately predict the threshold stress intensity, $K_{ISCC\text{-}LT}$, for AH and BH Alloy X-750 under increasing load conditions and conservatively predict it for constant-load conditions, low-rate rising load testing in high hydrogen water is an effective and appropriate method for determining $K_{ISCC\text{-}LT}$. For Condition HTH, rising load K_{Pmax} values provide a reasonable, but not necessarily conservative, estimate of $K_{ISCC\text{-}LT}$. To establish conservative $K_{ISCC\text{-}LT}$ values for these materials, crack arrest testing of multiple self-loaded specimens cooled from elevated temperatures should be performed.

It is noteworthy that low temperature cracking does not initiate in a reasonable length of time from a smooth surface or notch. A crack or crack-like defect must be present. As-notched configurations resist LTCP because the peak stresses and degree of hydrogen enrichment are much less severe than in precracked specimens. A key factor is the relatively large diffusional distance from the metal/water interface at the notch tip to the peak triaxial stress region which allows greater loss of hydrogen to the surrounding matrix.

While stress corrosion cracks cannot initiate at a notch in low temperature water, they can initiate and propagate in high temperature water at relatively low stresses and K_I levels. Hence, the failure process for Alloy X-750 involves crack initiation and growth by HTSCC or fatigue, and when a critical flaw size is reached, as defined by $K_{ISCC\text{-}LT}$, rapid low temperature cracking quickly leads to unstable fracture during cooldown.

Figure 21 shows that PSES provides a reasonable correlation of HTSCC initiation times and the stress exponents, n, were -0.8 and -1.4 for Conditions AH and HTH, respectively. Initiation times for Condition HTH are two to three orders of magnitude greater than those for Condition

AH at PSES values above 2760 MPa. The difference is probably greater at lower stresses due to the higher stress exponent for the former.

The HTH treatment also improves resistance to SCC incubation and growth. Crack incubation times for precracked AH and HTH samples differed by two to three orders of magnitude and SCC rates differed by one to two orders of magnitude. Activation energies for crack incubation (62 and 66 kcal/mol) and crack growth rates (34 and 41 kcal/mol) were relatively insensitive to heat treatment. These high activation energies indicate that the rate controlling processes for SCC are different in the low and high temperature regimes. At high temperatures, a hydrogen-assisted cracking mechanism is believed to be operative, but the controlling mechanism is probably a thermally activated slip process.

The superior HTSCC performance of Condition HTH materials is believed to be associated with reduced phosphorus segregation, reduced γ' and an absence of MC carbides decorating the grain boundaries,[1, 27, 28] a high density of intergranular $M_{23}C_6$ carbides[1-3, 26] and a larger grain size.[29] The γ' phase that decorates AH grain boundaries plays a dual role: it is highly anodic which results in hydrogen generation at the cathodic matrix[26, 28] and it is a strong hydrogen trap.[30] The HTH treatment reduces the amount of intergranular γ' and increases the amount of $M_{23}C_6$, which is cathodic with respect to the matrix. The reduction of intergranular γ' enhances corrosion resistance and minimizes hydrogen pickup. The larger grain size is believed to improve SCC performance by increasing the characteristic distance over which critical levels of hydrogen and strain energy density must be attained to cause SCC.[29] Moreover, modification of the grain boundary structure by grain coarsening is critical to minimizing phosphorus segregation during the subsequent aging treatment.

CONCLUSIONS

Stress corrosion cracking tests were performed on as-notched and precracked specimens of Conditions AH, BH and HTH Alloy X-750 in low and high temperature water. Operative cracking mechanisms were characterized by comparing the cracking response in water with that for hydrogen-precharged specimens tested in air. In addition, Auger analyses were performed to relate grain boundary segregation to SCC performance. The conclusions are given below:

1. Regardless of heat treatment, Alloy X-750 is susceptible to rapid cracking in low temperature water, with growth rates as high as 7 mm/min. Stress intensity factors associated with LTCP are a fraction of K_{Ic} levels in air, thereby negating the inherent high fracture resistance of this material.

2. The low temperature cracking phenomenon is associated with embrittlement of grain boundaries by hydrogen generated by the corrosion reaction at a crack tip. Hydrogen diffuses to the peak triaxial stress region ahead of the crack, and a three to four-fold enrichment can occur below 100°C. Comparison of K_{Pmax} values for non-precharged specimens tested in water with those for hydrogen-precharged specimens tested in air indicates that the critical hydrogen concentration to produce LTCP is on the order of 100 ppm. The equivalence of activation energies for Stage II crack growth rates (11.3 kcal/mol) and hydrogen diffusion (11.5 kcal/mol) demonstrates that hydrogen diffusion is the rate controlling process for LTCP.

3. Hydrogen in the water, which increases equilibrium nascent hydrogen at the water-metal interface, reduces LTCP resistance. Hence, the hydrogen content of the water should be reduced below 20 cc H_2/kg H_2O whenever the water temperature is below 150°C to minimize the potential for LTCP.

4. Variability in LTCP resistance is correlated with the degree of phosphorus and sulfur segregation to grain boundaries. Grain coarsening associated with the high temperature HTH anneal produces a grain boundary structure that dramatically decreases the tendency for phosphorus segregation during subsequent aging at 704°C. As grains coarsen, small intergranular niobium and titanium carbides dissolve and subsequent aging during the HTH treatment induces chromium-rich $M_{23}C_6$ carbides to form on grain boundaries. The

increased matrix niobium and titanium is believed to react with phosphorus to retard segregation. In fine grained AH and BH materials, grain boundaries are decorated with niobium and titanium carbides, so reduced amounts of these elements are available to tie up phosphorus.

5. In HTH materials, reduced grain boundary sulfur resulted in superior LTCP properties. Since decreased sulfur segregation is correlated with reduced bulk content, improved ingot microcleanliness provides superior low temperature cracking performance.

6. For materials with low and intermediate LTCP resistance, K_{Pmax} values obtained from conventional rising load tests provide a conservative estimate of the critical stress intensity factor ($K_{ISCC\text{-}LT}$) for rapid low temperature cracking regardless of the load path that occurs during cooldown. For highly resistant materials (K_{Pmax} > 45 MPa$\sqrt{m}$), rising load tests provide a reasonable, but not necessarily conservative, estimate of $K_{ISCC\text{-}LT}$. For these materials, crack arrest testing of bolt-loaded specimens is the most effective method for conservatively determining $K_{ISCC\text{-}LT}$.

7. LTCP will initiate from a crack-like defect, but not from a smooth surface or notch because the peak stresses and degree of hydrogen enrichment are much less severe. Thus, the failure scenario for Alloy X-750 involves crack initiation and growth by HTSCC or fatigue, followed by LTCP when a critical flaw size is reached.

8. Above 150°C, the degree of hydrogen enrichment decreases and the fracture resistance of grain boundaries in the presence of hydrogen increases significantly; hence, the rapid cracking phenomenon does not occur. Stress corrosion cracking does occur between 288° and 360°C, but cracking rates are orders of magnitude slower than LTCP rates. At elevated temperatures, the high activation energies for crack incubation (62 and 66 kcal/mol) and growth rates (33.8 and 41 kcal/mol) indicate that the controlling mechanism is a thermally activated slip process, rather than hydrogen diffusion.

9. The HTSCC performance for Condition HTH is far superior to that for Condition AH. Crack initiation times for HTH heats are typically three orders of magnitude greater than in AH heats, and crack growth rates are one to two orders of magnitude lower. The superior performance of HTH materials is believed to be associated with reduced phosphorus

segregation, reduced intergranular γ' which is highly anodic and serves as a strong hydrogen trap, a large grain size and a high density of intergranular $M_{23}C_6$ carbides, rather than niobium and titanium-rich MC-type carbides.

Acknowledgement

This work was performed under U. S. Department of Energy Contract DE-AC11-93PN38195 with Bettis Atomic Power Laboratory, a unit of Westinghouse Electric Corporation.

THIS PAGE IS INTENTIONALLY BLANK

REFERENCES

1. C. A. Grove and L. D. Petzold, "Mechanisms of Stress-Corrosion Cracking of Alloy X-750 in High-Purity Water," Journal of Materials for Energy Systems, Vol. 7, 1985, pp. 147-162.

2. I. L. W. Wilson and T. R. Mager, "Stress Corrosion of Age-Hardenable NiCrFe Alloys," Corrosion, Vol. 42, 1986, pp. 352-361.

3. M. T. Miglin and H. A. Domian, "Microstructure and Stress Corrosion Resistance of Alloys X750, 718 and A286 in Light Water Reactor Environments," Journal of Materials Engineering, Vol. 9, 1987, pp. 113-132.

4. A. A. Stein, "Proceedings: 1986 Workshop on Advanced High-Strength Materials," EPRI Report NP-6363, Edited by M. S. Gennaro and J. L. Nelson, May 1989.

5. A. R. McIlree, "Degradation of High Strength Austenitic Alloys X-750, 718, and A-286 in Nuclear Power Systems," International Symposium on Environmental Degradation of Materials in Nuclear Power Systems-Water Reactors, Myrtle Beach, SC, August 1983, pp. 838-850.

6. G. O. Hayner and R. G. Ballinger, "Nickel Chromium Iron Alloys for Nuclear Reactor Vessel Components," EPRI Report NP-5429M, October 1987.

7. W. J. Mills, M. R. Lebo, J. J. Kearns, R. C. Hoffman, J. J. Korinko, R. F. Luther and G. B. Sykes, "Effect of Irradiation on the Stress Corrosion Cracking Behavior of Alloy X-750 and Alloy 625," Sixth International Symposium on Environmental Degradation of Materials in Nuclear Power Systems - Water Reactors, TMS, 1993, pp. 633-643.

8. A. Saxena and S. J. Hudak, Jr., "Review and Extension of Compliance Information for Common Crack Growth Specimens," International Journal of Fracture, Vol. 14, 1978, pp. 453-468.

9. J. Crank, The Mathematics of Diffusion, Oxford University Press, London, 1956.

10. W. J. Mills, "Effect of Temperature on the Fracture Toughness Behavior of Inconel X-750, "Fractography and Materials Science, ASTM STP 733, 1981, pp. 98-114.

11. D. M. Symons, "An Investigation into the Effects of Hydrogen on the Fracture and Deformation Behavior of Alloy X-750," Ph.D. Disertation, Carnegie Mellon University, Pittsburgh, PA, 1994.

12. W. M. Robertson, "Hydrogen Permeation and Diffusion in Inconel 718 and Incoloy 903," Metallurgical Transactions, Vol. 8A, 1977, pp. 1709-1712.

13. R. M. Latanision and M. Kurkela, "Hydrogen Permeability and Diffusivity in Nickel and Ni-Base Alloys," Corrosion, Vol. 39, 1983, pp. 174-180.

14. W. W. Gerberich and Y. T. Chen, "Hydrogen-Controlled Cracking-An Approach to Threshold Stress Intensity, "Metallurgical Transactions, Vol. 6A, 1975, pp. 271-278.

15. B. B. Baranowski, S. Majchrzak and T. B. Flanagan, "The Volume Increase of FCC Metals and Alloys Due to Interstitial Hydrogen Over a Wide Range of Hydrogen Contents," Journal of Physics F: Metal Physics, Vol. 1, 1971, pp. 258-261.

16. M. L. Wayman and G. C. Smith, "Hydride Formation in Nickel-Iron Alloys," The Journal of Physics and Chemistry of Solids, Vol. 32, 1971, p. 103.

17. R. A. Oriani, "On the Partial Molal Volume of Hydrogen in Alpha Iron," Transactions of the Metallurgical Society of AIME, Vol. 236, 1966, pp. 1368-1369.

18. J. R. Rice, "Note: Some Mechanics Research Topics Related to the Hydrogen Embrittlement of Metals," Corrosion, Vol. 32, 1976, pp. 22-26.

19. W. W. Gerberich, T. Livne, X. F. Chen and M. Kaczorowski, "Crack Growth from Internal Hydrogen-Temperature and Microstructural Effects in 4340 Steel," Metallurgical Transactions, Vol. 19A, 1988, pp. 1319-1334.

20. R. Moller and H. J. Grabke, Grain Boundary Segregation of Phosphorus in Fe-Nb-P and Fe-Nb-C-P Alloys," Scripta Metallurgica, Vol. 18, 1984, pp. 527-530.

21. R. D. K. Misra, C. Y. Prasad, T. V. Balasubramanian and P. Rama Rao, "Effect of Phosphorus Segregation on Impact Toughness Variation in 17-4 Precipitation Hardened Stainless Steel," Scripta Metallurgica, Vol. 20, 1986, pp. 713-716.

22. M. Creager and P. C. Paris, "Elastic Field Equations for Blunt Cracks with Reference to Stress Corrosion Cracking," International Journal of Fracture Mechanics, Vol. 3, 1967, pp. 247-252.

23. W. K. Wilson, "Elastic-Plastic Analysis of Blunt Notched CT Specimens and Applications," Journal of Pressure Vessel Technology, 1974, Vol. 96, pp. 293-298.

24. G. Glinka, "Calculation of Inelastic Notch-Tip Strain-Stress Histories Under Cyclic Loading," Engineering Fracture Mechanics, Vol. 22, 1985, pp. 839-854.

25. Y. Shen and P. G. Shewmon, "IGSCC Crack Growth of Alloy 600 and X-750 in Steam," Corrosion, Vol. 47, 1991, pp. 712-718.

26. K. Hosoya, R. Ballinger, J. Prybylowski and I. S. Hwang, "Microstructural Role in Environmentally Assisted Cracking of Ni-Base Alloys," Corrosion, Vol. 44, 1988, pp. 838-852.

27. R. G. Ballinger, C. K. Elliott and I. S. Hwang, "Corrosion Fatigue of Alloy X-750 in Aqueous Environment," Proceedings of the First International Conference on Environmental-Induced Cracking of Metals, (NACE), 1988, pp. 241-249.

28. I. S. Hwang, R. G. Ballinger, J. W. Prybylowski and K. Hosoya, "Electrochemistry of Multiphase Nickel-Base Alloys in Aqueous Systems," Journal of the Electrochemical Society, Vol. 136, 1989, pp. 1874-1883.

29. M. M. Hall, Jr., D. M. Symons and J. J. Kearns, "Strain Energy Density-Distance Criterion for the Initiation of Hydrogen-Induced Cracking of Alloy X-750," Parkins Symposium on Fundamental Aspects of Stress Corrosion Cracking, TMS, 1992, pp. 231-244.

30. A. Turnbull, R. G. Ballinger, I. S. Hwang and R. M. Gates, "The Influence of Microstructure on Hydrogen Transport in Nickel-Base Alloys," Proceedings of the Fourth International Conference on Hydrogen Effects on Material Behavior, TMS, 1990, pp. 121-139.

Table 1
Heat Treatment Conditions

Condition AH

Hot worked
Stress equalized at 885°C for 24 hours, air cooled
Aged at 704°C for 20 hours, air cooled

Condition BH

Hot worked
Aged at 704°C for 20 hours, air cooled

Condition HTH

Hot worked
Annealed at 1093°C for 1 hour, air cooled
Aged at 704°C for 20 hours, air cooled

Table 2
Chemical Composition of Test Materials (in weight percent)

Heat[1]	Cond.	Ni	Cr	Fe	Ti	Nb/Ta	Al	Mn	Si	C	Co	Cu	V	P	S	B
A2	HTH	71.88	15.54	7.98	2.65	1.05	0.68	0.10	0.03	0.043	0.02	0.09	0.01	0.002	0.0001	0.0027
A6	HTH	70.70	15.04	7.90	2.58	1.01	0.75	0.06	0.07	0.040	0.01	0.02	0.02	0.001	0.001	0.0026
A17	HTH	71.62	15.63	8.04	2.63	1.04	0.68	0.13	0.04	0.040	0.01	0.03	0.02	0.001	0.0002	NA[2]
A18	HTH	71.02	15.19	7.79	2.58	1.04	0.70	0.19	0.09	0.041	0.01	0.05	0.02	0.001	0.0002	NA
A9	HTH	71.22	15.49	7.70	2.66	1.02	0.73	0.11	0.06	0.037	0.01	0.01	0.06	0.004	0.003	<0.001
A10	HTH	71.17	15.46	8.33	2.67	1.00	0.77	0.10	0.11	0.072	0.07	0.01	0.02	0.007	0.001	0.0070
A13	HTH	70.97	15.63	8.25	2.66	1.00	0.77	0.09	0.07	0.067	0.05	0.01	0.03	0.003	0.002	NA
A14	HTH	72.00	15.59	8.29	2.67	1.00	0.80	0.09	0.12	0.066	0.05	0.01	0.02	0.008	0.002	NA
A15	HTH	71.22	15.65	7.97	2.57	1.01	0.72	0.08	0.02	0.040	0.01	0.01	0.02	0.001	0.003	<0.001
A16	HTH	72.62	15.77	8.01	2.68	1.07	0.68	0.15	0.03	0.064	0.07	0.03	0.02	0.007	0.002	0.007
B1	HTH	71.73	15.52	8.41	2.42	0.89	0.63	0.05	0.06	0.05	0.02	0.01	0.02	0.005	0.005	0.0045
B3	HTH*[3]	NA	NA	NA	NA	NA	NA	NA	NA	NA	NA	NA	NA	NA	NA	NA
B8	HTH*	70.68	16.10	8.03	2.73	0.89	0.80	0.14	0.10	0.033	0.11	0.12	0.17	0.008	0.0015	0.003
B9	HTH	71.98	15.54	8.24	2.56	0.86	0.78	0.03	0.05	0.041	0.05	0.01	0.04	0.005	0.001	NA
B2	BH	71.35	15.31	8.26	2.66	0.85	0.85	0.15	0.09	0.029	0.04	0.01	NA	NA	0.002	NA
B4	BH,HTH*	71.17	15.69	8.54	2.56	0.87	0.80	0.11	0.11	0.03	0.04	0.05	NA	0.0057	0.002	NA
B5	BH,HTH*	71.86	16.65	7.58	2.62	0.86	0.83	0.04	0.08	0.03	0.02	0.01	NA	NA	0.003	NA
B6	BH	71.39	15.42	7.91	2.51	0.95	0.84	0.14	0.10	0.026	0.02	0.01	NA	NA	0.005	NA
B7	BH	72.37	15.41	7.52	2.66	0.86	0.88	0.04	0.08	0.06	0.01	0.02	NA	NA	0.003	NA
C2	BH,HTH*	72.36	15.74	7.08	2.50	0.98	0.70	0.13	0.08	0.05	0.08	0.04	NA	0.004	0.004	NA
D3	BH,HTH*	72.03	15.53	7.22	2.51	0.99	0.83	0.24	0.50	0.03	0.04	0.12	NA	NA	0.004	NA

D4[4]	BH	74.01	15.14	6.26	2.53	0.95	0.78	0.09	0.17	0.06	NA	0.01	NA	0.0095	0.004	NA
D5	BH	72.13	15.53	7.22	2.51	0.99	0.83	0.26	0.09	0.03	0.05	0.15	0.19	0.0073	0.004	0.003
D6	BH,AH	71.16	16.60	7.43	2.31	0.99	0.74	0.24	0.30	0.06	NA	0.16	NA	0.0023	0.005	NA
D7	AH	72.62	15.86	6.77	2.53	0.88	0.77	0.16	0.26	0.04	0.06	0.08	NA	NA	0.007	NA
D8	AH	70.56	16.03	8.23	2.48	1.03	0.69	0.32	0.11	0.05	0.10	0.20	0.18	0.009	0.0007	0.002
D9	AH	70.76	16.31	7.76	2.50	0.98	0.80	0.27	0.31	0.05	0.04	0.26	NA	NA	0.004	NA
D10	AH	73.63	15.44	6.75	2.49	0.96	0.77	0.08	0.11	0.03	0.04	0.01	NA	NA	0.007	NA
E1	AH	71.41	16.34	7.12	2.73	1.04	0.50	0.21	0.10	0.06	0.21	0.025	0.23	0.006	0.0006	0.002

1. The letter denotes Vendor A, B, C, D or E.

2. NA = Not Available

3. Asterisk denotes material was given the BH treatment followed by the HTH treatment. This is assumed to be equivalent to the conventional HTH treatment because the high temperature anneal should remove the effects of the BH treatment.

4. Two sections from this heat were subjected to different thermomechanical processing histories. One was hot rolled at 982°C and the other at 1093°C.

Table 3
Tensile Properties at Room Temperature

Condition	Yield Strength (MPa)	Ultimate Strength (MPa)	Elongation (%)	Reduction in Area (%)	Rockwell Hardness Rc
AH	823 ± 57	1227 ± 32	24 ± 2.5	38 ± 4.5	35 ± 1.7
BH	985 ± 77	1325 ± 50	23 ± 2.1	41 ± 3.4	38 ± 2.3
HTH	792 ± 20	1196 ± 15	27 ± 1.7	35 ± 4.8	32 ± 1.4

Figure Captions

Figure 1. Typical microstructures: (a) Condition AH Heat D6, (b) Condition BH Heat D6 and (c) Condition HTH Heat A6.

Figure 2. Rising load test results for BH Heat B4 in 93°C air and argon-sparged water. Tests were performed on three-point-bend specimens at a displacement rate of 0.05 mm/min. SEM fractographs show dimple rupture mechanism operative in air and intergranular cracking mechanism operative in water.

Figure 3. Effect of temperature on K_{Pmax} values for (a) AH, (b) BH and (c) HTH heats. Solid symbols denote specific heats tested in both the BH and HTH conditions. The broken and solid lines represent lower bound curves for 16 cc H_2/kg H_2O and 35-60 cc H_2/kg H_2O water. Arrows indicate the range of K_{Pmax} values in air.

Figure 4. Effect of hydrogen content of water on the minimum K_{Pmax} (or arrest $K_{ISCC\text{-}LT}$ for Heat A6) observed below 150°C. The solid symbols denote those heats tested in both the BH and HTH conditions. K_{Pmax} values obtained in argon-sparged 93°C water (i.e., 0 cc H_2/kg H_2O) are also shown for comparison.

Figure 5. Resistance to LTCP during continuous cooling under constant-load conditions. Precracked CT specimens were heated to 288°C, loaded and then cooled under constant load. Open circles indicate no cracking during continuous cooling, 'X' corresponds to rising load K_{Pmax} after cooldown tests and solid lines represent isothermal rising load K_{Pmax} loci.

Figure 6. LTCP induced by mildly increasing loads during continuous cooling from 288°C. Closed circles denote LTCP, open circles denote survivors, broken lines represent K_I versus temperature path during continuous cooling and solid lines represent isothermal rising load K_{Pmax} loci.

Figure 7. Agreement in rising load K_{Pmax} and critical LTCP stress intensities ($K_{ISCC\text{-}LT}$) based on constant-displacement and constant-load tests. Specimens in constant-load tests saw no high temperature water exposure. LTCP occurred in times as short as 2 days and as long as 60 days; all constant-load survivors were exposed for one year.

Figure 8. Temperature dependence of Stage II crack growth rates for BH Heat B5 in argon-sparged deionized water. ($R = 1.987$ cal K^{-1} mol^{-1})

Figure 9. Typical fracture surface morphologies observed in the low temperature regime.
(a) Non-precharged specimen tested in air showing ductile microvoid coalescence.
(b) Non-precharged specimen tested in water showing intergranular cracking.
(c) Hydrogen-precharged specimen tested in air showing intergranular appearance that is indistinguishable from LTCP fracture surface morphology shown in (b).

Figure 10. Comparison of hydrogen diffusion coefficients in Alloy X-750 and Alloy 718. ($R = 1.987$ cal K^{-1} mol^{-1})

Figure 11. Individual and combined effects of precharged hydrogen and hydrogen picked up in low temperature water with 16 cc H_2/kg H_2O. (a) AH specimens were tested in both the precracked and as-notched configurations. (b) BH and (c) HTH specimens were precracked prior to testing.

Figure 12. Effect of temperature and yield strength (σ_{YS}) on calculated maximum hydrogen enrichment in the peak triaxial stress region ahead of a crack in Alloy X-750.

Figure 13. Hydrogen dependence of K_{Pmax} for precracked specimens from BH Heats B7 and D6 that were hydrogen precharged and tested in 24° and 93°C air. The solid line shows the correlation of K_{Pmax} with the measured bulk hydrogen content for fast tests (solid symbols) and calculated local hydrogen enrichment for slow tests (partially closed symbols). The low toughness exhibited in the fast test of the B7 specimen containing 56 ppm hydrogen is attributed to data scatter.

Figure 14. Temperature dependence of K_{Pmax} for precracked specimens that were hydrogen precharged and tested in air. Elevated temperature test times were minimized to preclude significant hydrogen loss.

Figure 15. Fracture surface morphology for hydrogen-precharged specimen tested in 288°C air.
(a) Mixed mode fracture with approximately equal amounts of intergranular and transgranular cracking.
(b) High magnification of center region of (a) showing transgranular facets associated with a channel fracture mechanism.

Figure 16. Illustration of difference in peak principal stress (σ_{yy}) and diffusion distance to assumed crack nucleation site for hydrogen released by corrosion reaction in precracked and as-notched specimens. Y direction is normal to the crack or notch plane.

Figure 17. As-notched specimen from BH Heat B4 tested in 88°C water showing a transgranular dimple rupture region between base of notch and intergranular region.

Figure 18. Correlation of rising load K_{Pmax} values in argon-sparged deionized water at 93°C with bulk and grain boundary phosphorus concentrations. LTCP resistance correlates with grain boundary phosphorus content, but not with bulk content. Heat identification is provided inside parenthesis.

Figure 19. Phosphorus segregation kinetics at 794°C in coarse and fine grain samples from Heat B4. Prior to 704°C aging, the fine grain material was annealed at 954°C whereas a 1121°C anneal was used to produce a coarse grain structure.

Figure 20. Correlation of rising load K_{Pmax} values in argon-sparged 93°C water with grain boundary sulfur and phosphorus concentrations. Grain boundary sulfur correlates with variability in K_{Pmax} values for BH and HTH heats. While lower grain boundary phosphorus accounts for the overall improvement in LTCP resistance for Condition HTH, it does not correlate with heat-to-heat variations. Heat identification and bulk sulfur and phosphorus contents are provided parenthetically.

Figure 21. SCC initiation time in 360°C water as a function of PSES for as-notched CT specimens from AH Heat D8 and HTH Heat A6. Power-law correlations are based on maximum-likelihood analysis. Up arrows indicate absence of HTSCC.

Figure 22. K_I dependence of SCC incubation times for precracked CT specimens for five HTH heats.

Figure 23. Temperature dependence of SCC incubation times for precracked CT specimens from AH Heat D9 and HTH Heat A13. Open symbols with arrows denote absence of HTSCC.

Figure 24. Arrhenius plot of Stage II SCC rates for Condition AH Heats D6 and D7. ($R=1.987$ cal K^{-1} mol^{-1})

Figure 25. Temperature and K_I dependence of SCC rates for Condition HTH. ($R=1.987$ cal K^{-1} mol^{-1})

Figure 26. Intergranular fracture surface morphologies associated with HTSCC and hydrogen-precharged specimens tested in air are indistinguishable.
(a) SCC fracture surface for BH Heat B6 tested in 360°C water.
(b) Fracture surface for hydrogen-precharged BH Heat B6 tested in room temperature air.

THIS PAGE IS INTENTIONALLY BLANK

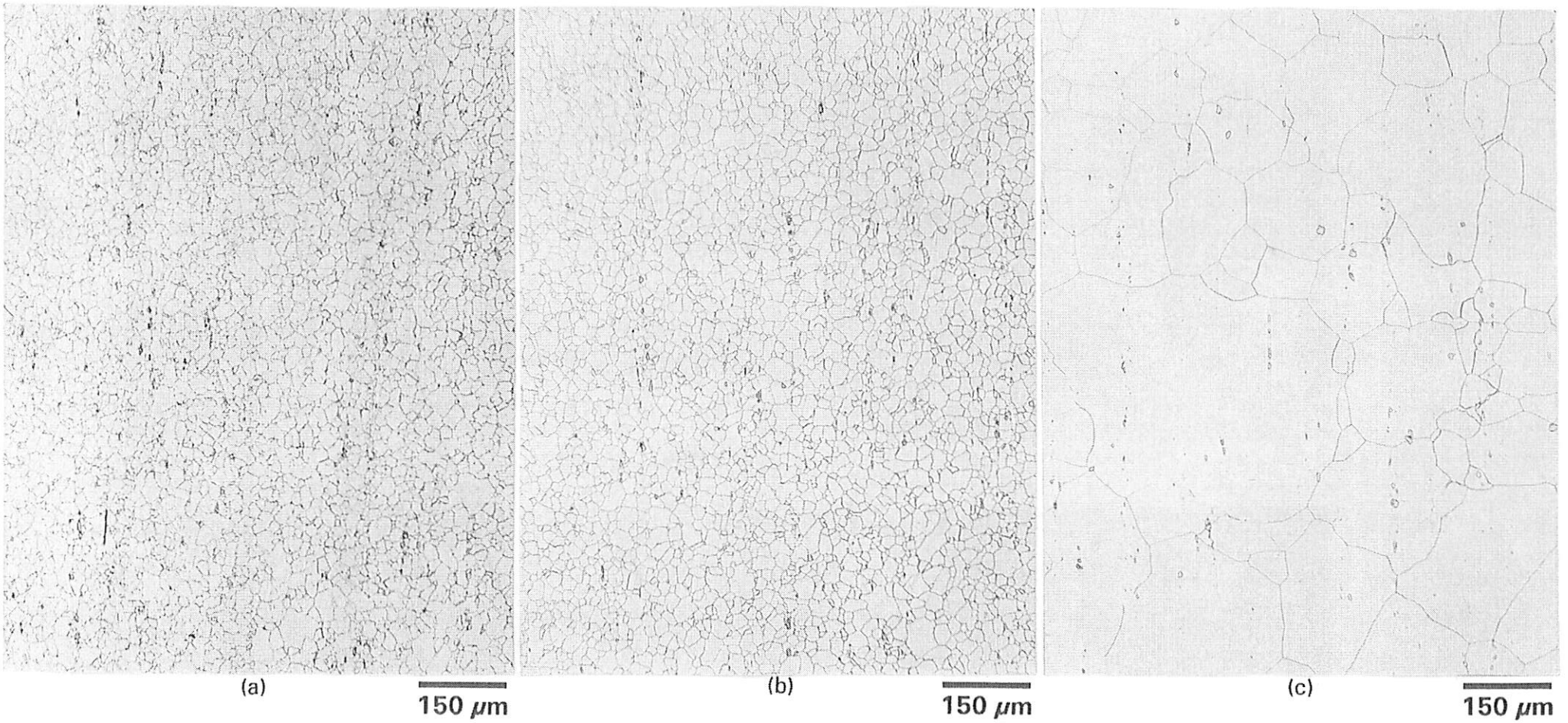

Figure 1. Typical microstructures: (a) Condition AH Heat D6, (b) Condition BH Heat D6 and (c) Condition HTH Heat A6.

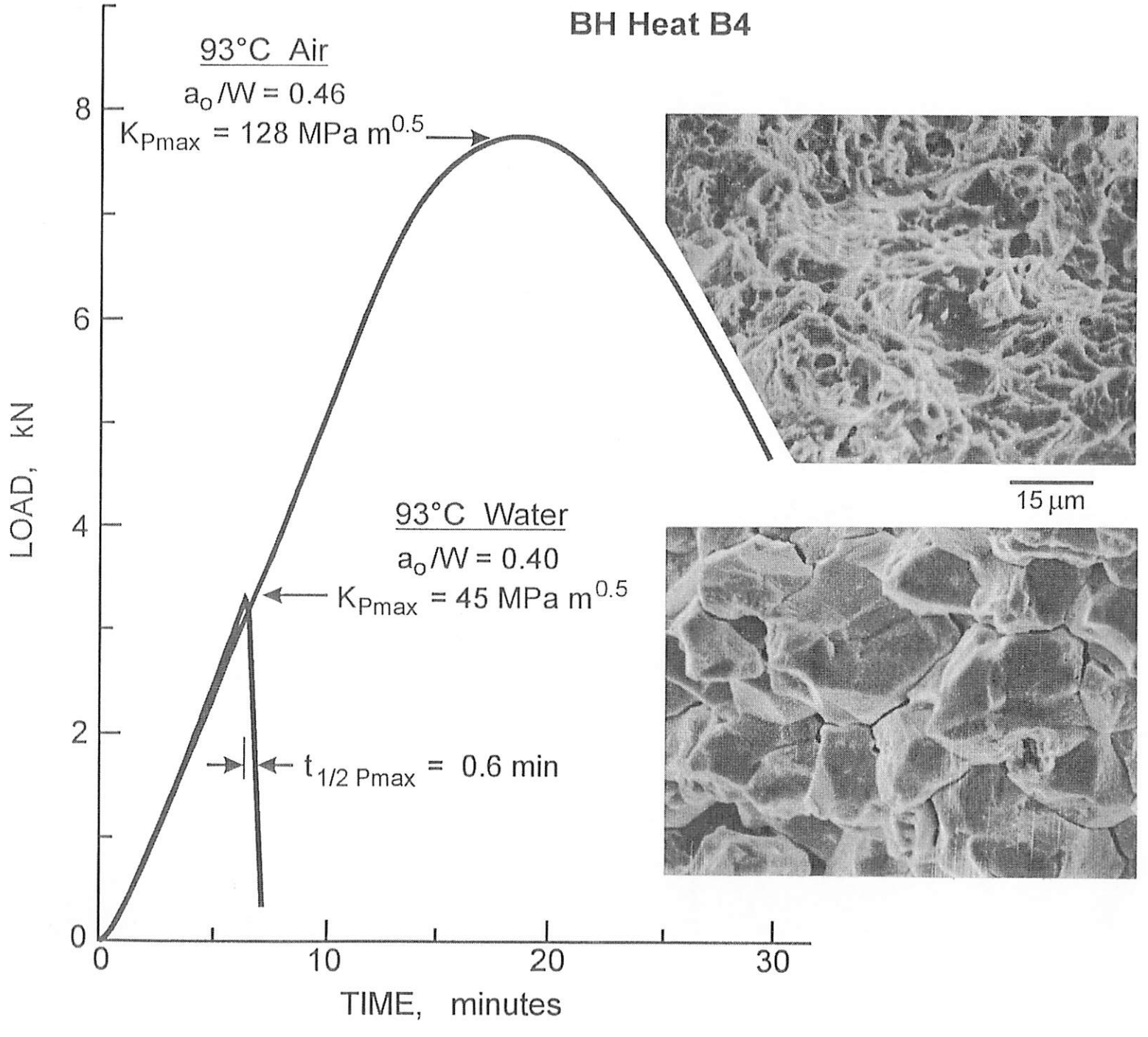

Figure 2. Rising load test results for BH Heat B4 in 93°C air and argon-sparged water. Tests were performed on three-point-bend specimens at a displacement rate of 0.05 mm/min. SEM fractographs show dimple rupture mechanism operative in air and intergranular cracking mechanism operative in water.

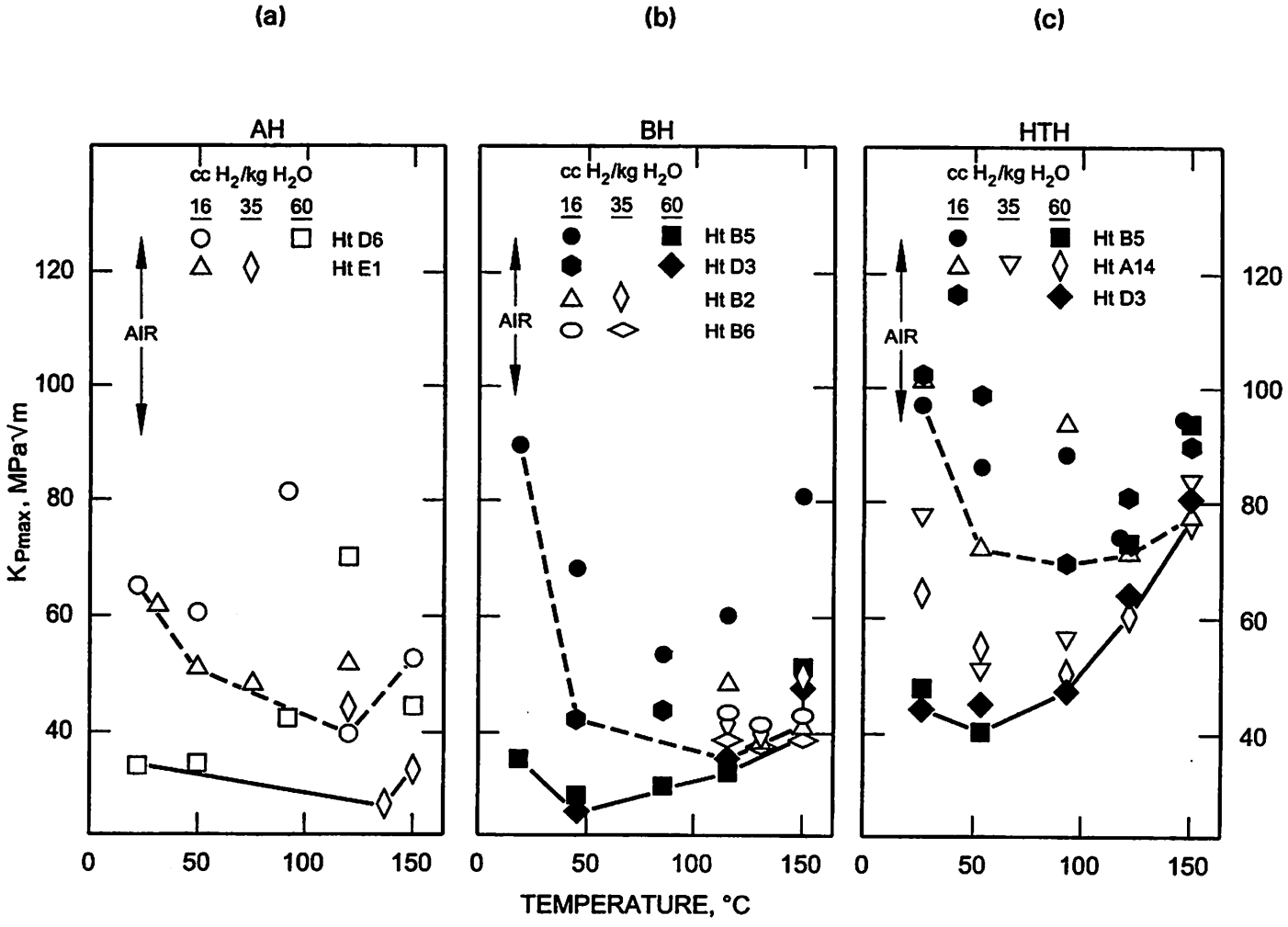

Figure 3. Effect of temperature on K_{Pmax} values for (a) AH, (b) BH and (c) HTH heats. Solid symbols denote specific heats tested in both the BH and HTH conditions. The broken and solid lines represent lower bound curves for 16 cc H_2/kg H_2O and 35-60 cc H_2/kg H_2O water. Arrows indicate the range of K_{Pmax} values in air.

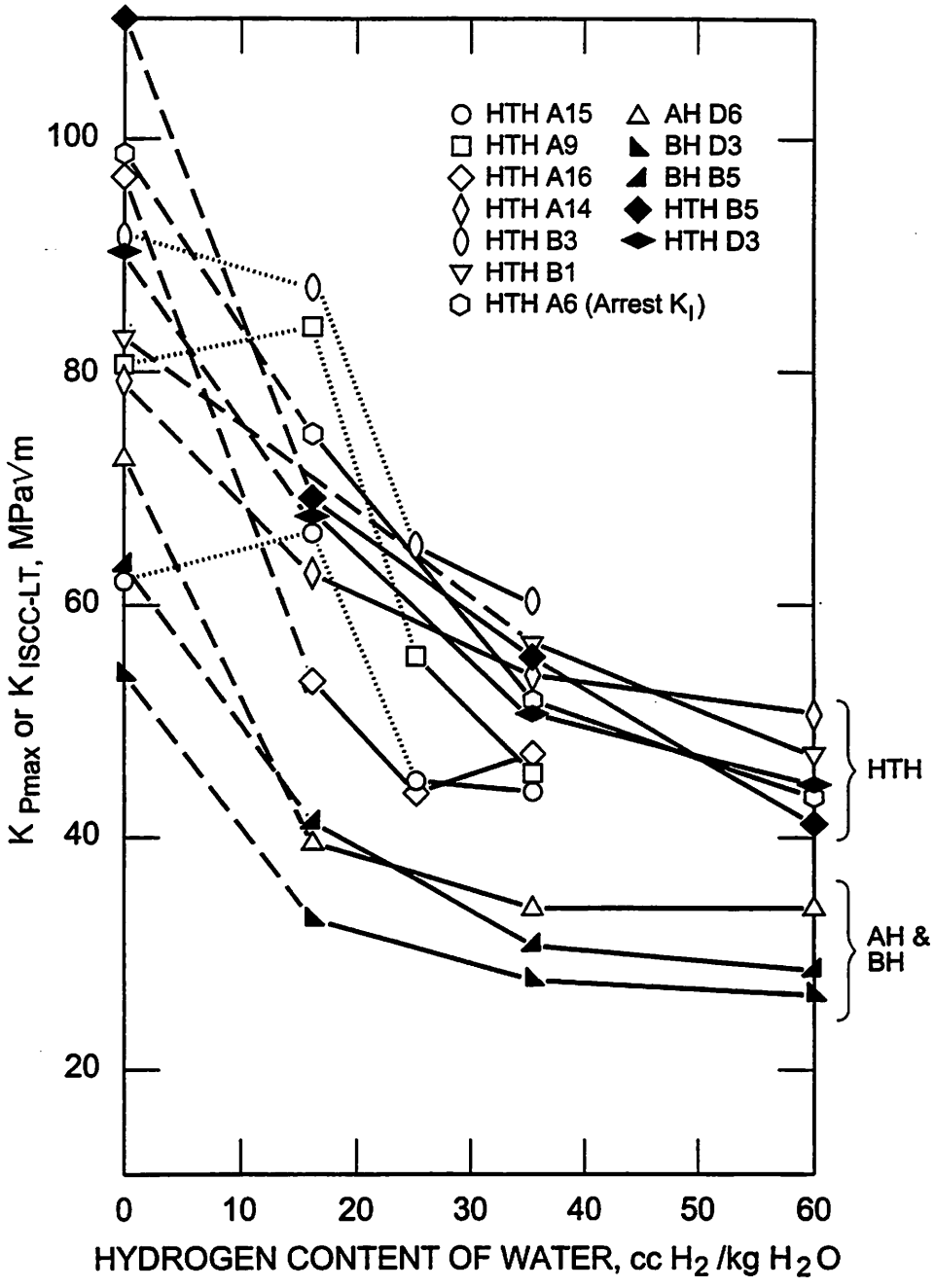

Figure 4. Effect of hydrogen content of water on the minimum K_{Pmax} (or arrest $K_{ISCC-LT}$ for Heat A6) observed below 150°C. The solid symbols denote those heats tested in both the BH and HTH conditions. K_{Pmax} values obtained in argon-sparged 93°C water (i.e., 0 cc H_2/kg H_2O) are also shown for comparison.

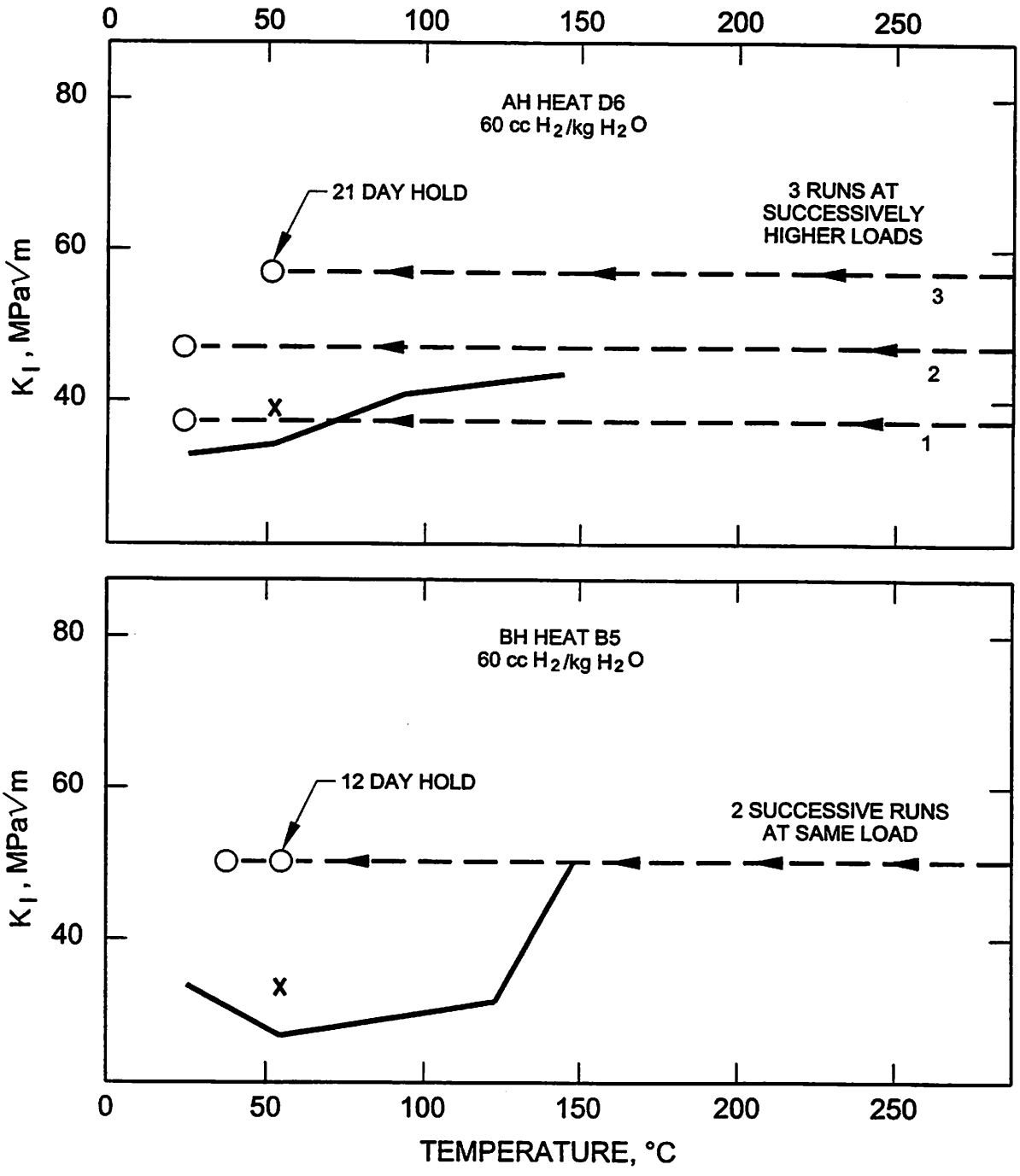

Figure 5. Resistance to LTCP during continuous cooling under constant-load conditions. Precracked CT specimens were heated to 288°C, loaded and then cooled under constant load. Open circles indicate no cracking during continuous cooling, 'X' corresponds to rising load K_{Pmax} after cooldown tests and solid lines represent isothermal rising load K_{Pmax} loci.

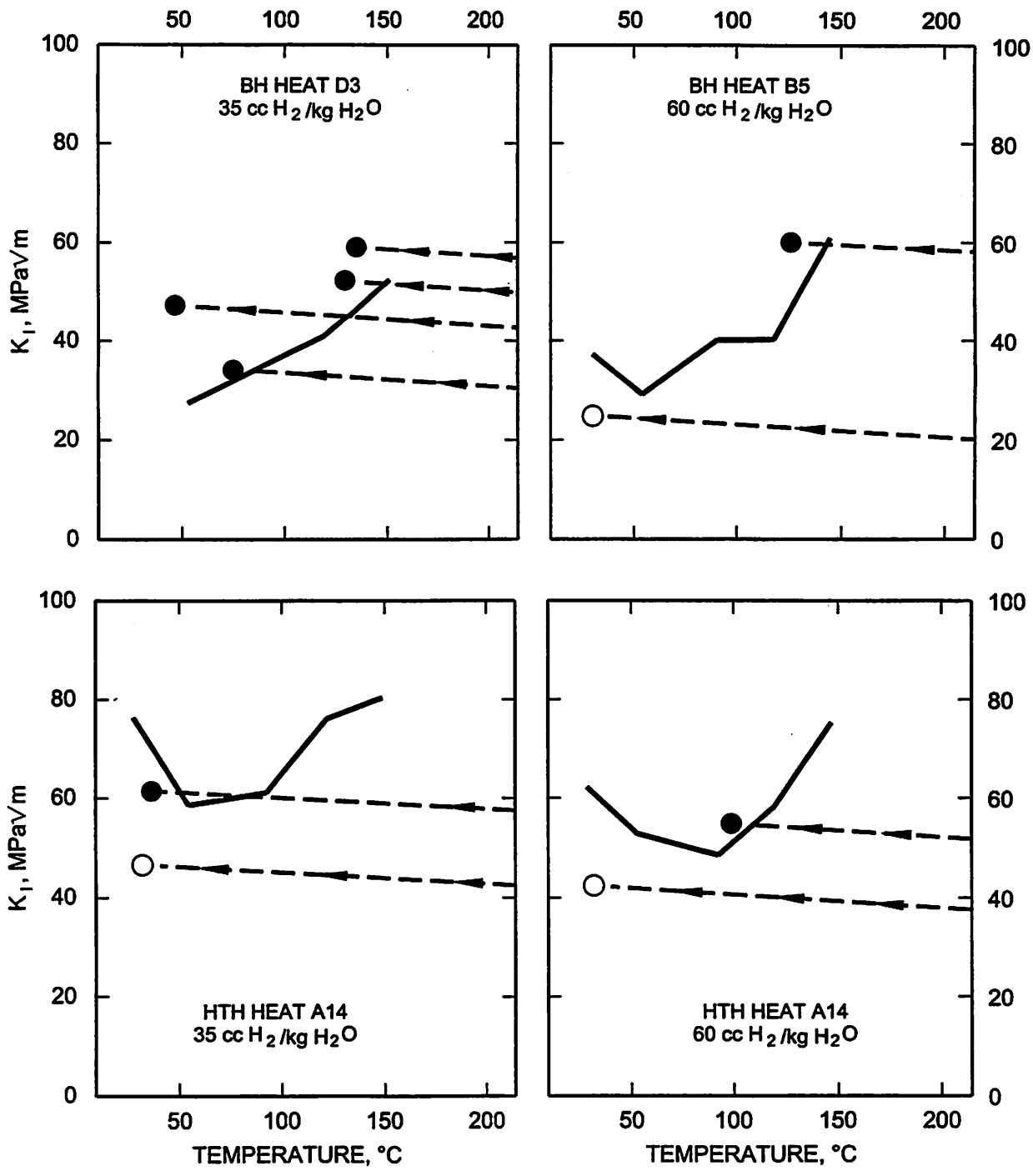

Figure 6. LTCP induced by mildly increasing loads during continuous cooling from 288°C. Closed circles denote LTCP, open circles denote survivors, broken lines represent K_I versus temperature path during continuous cooling and solid lines represent isothermal rising load K_{Pmax} loci.

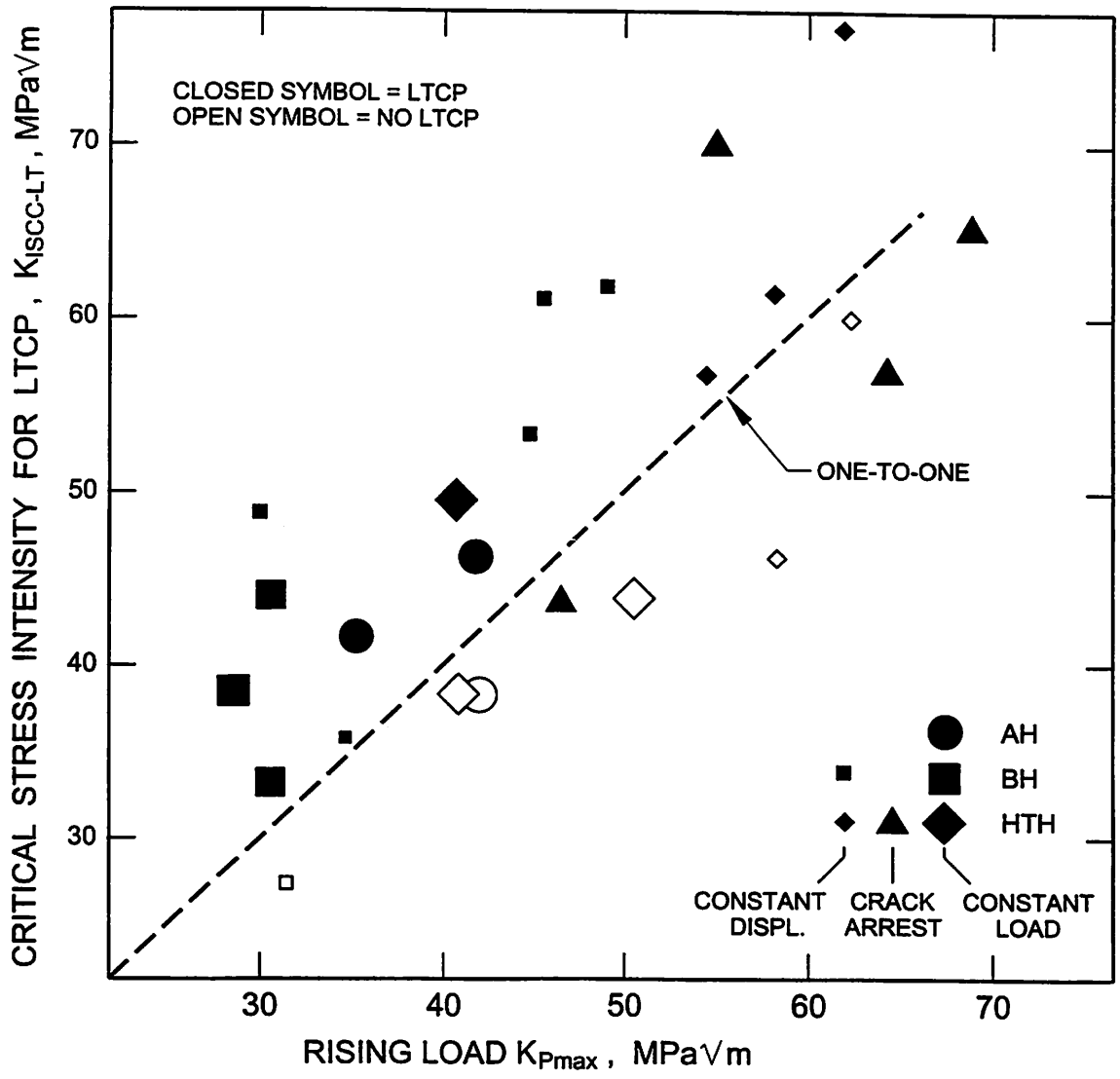

Figure 7. Agreement in rising load K_{Pmax} and critical LTCP stress intensities ($K_{ISCC-LT}$) based on constant-displacement and constant-load tests. Specimens in constant-load tests saw no high temperature water exposure. LTCP occurred in times as short as 2 days and as long as 60 days; all constant-load survivors were exposed for one year.

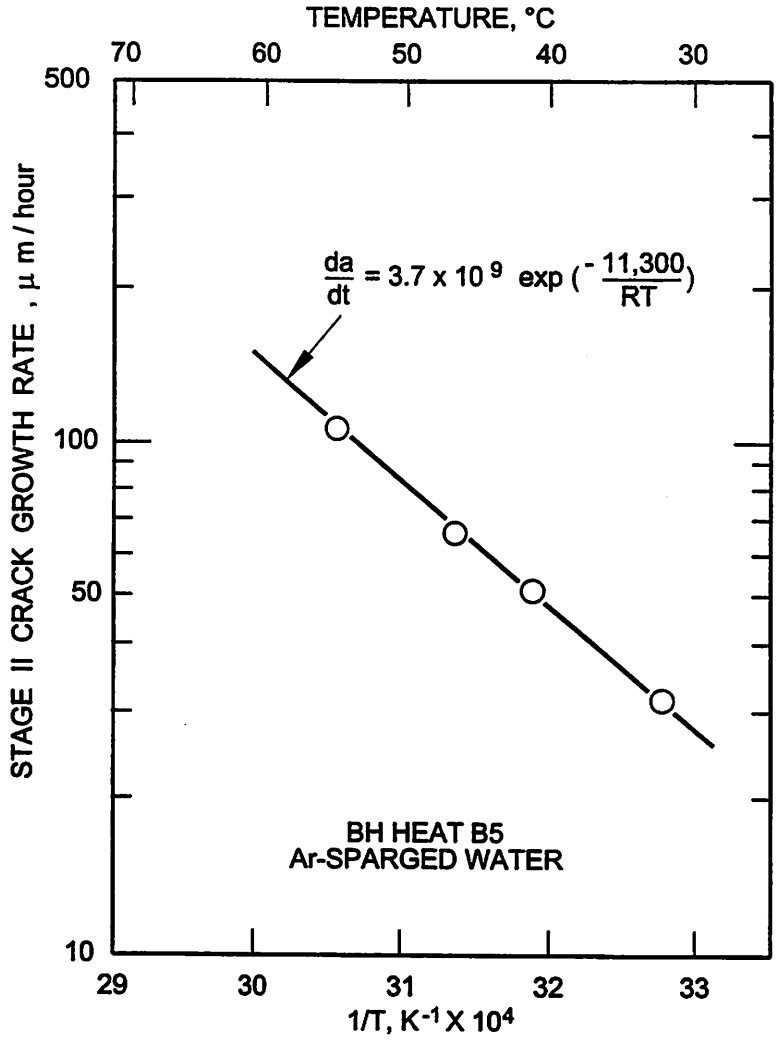

Figure 8. Temperature dependence of Stage II crack growth rates for BH Heat B5 in argon-sparged deionized water. (R = 1.987 cal K^{-1} $mole^{-1}$)

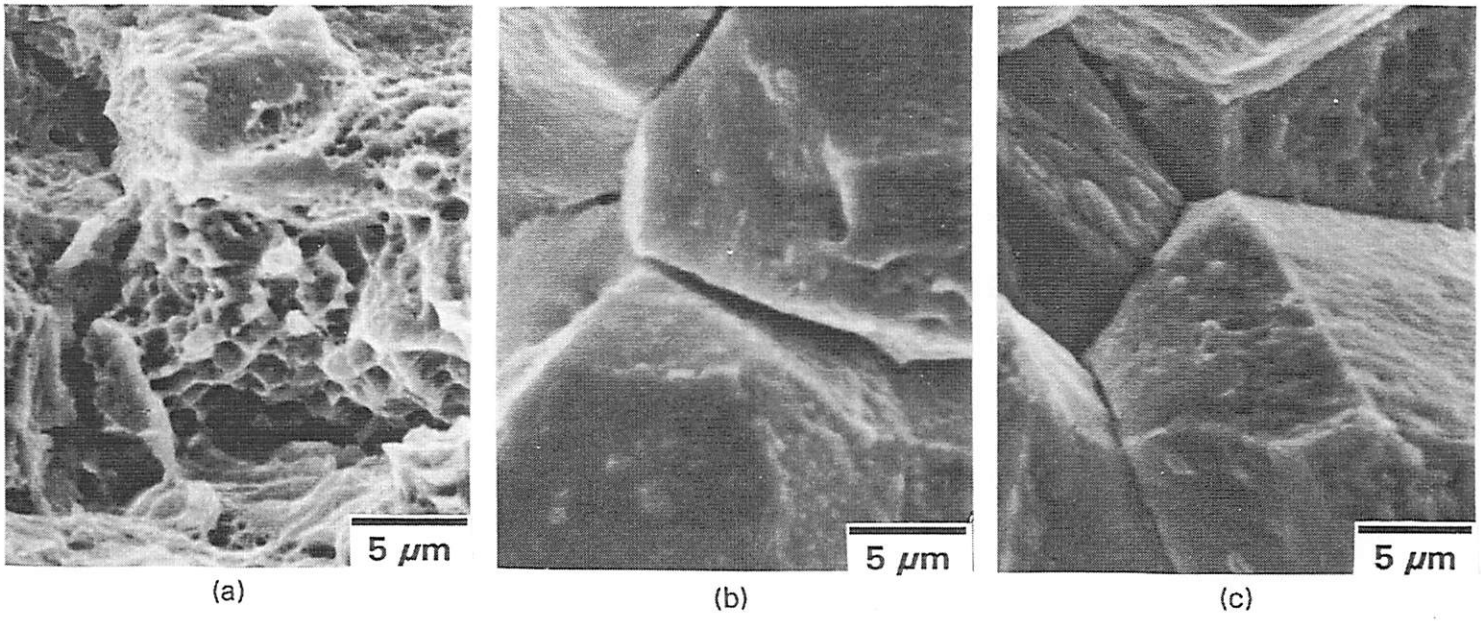

Figure 9. Typical fracture surface morphologies observed in the low temperature regime.
(a) Non-precharged specimen tested in air showing ductile microvoid coalescence.
(b) Non-precharged specimen tested in water showing intergranular cracking.
(c) Hydrogen-precharged specimen tested in air showing intergranular appearance that is indistinguisable from LTCP fracture surface morphology shown in (b).

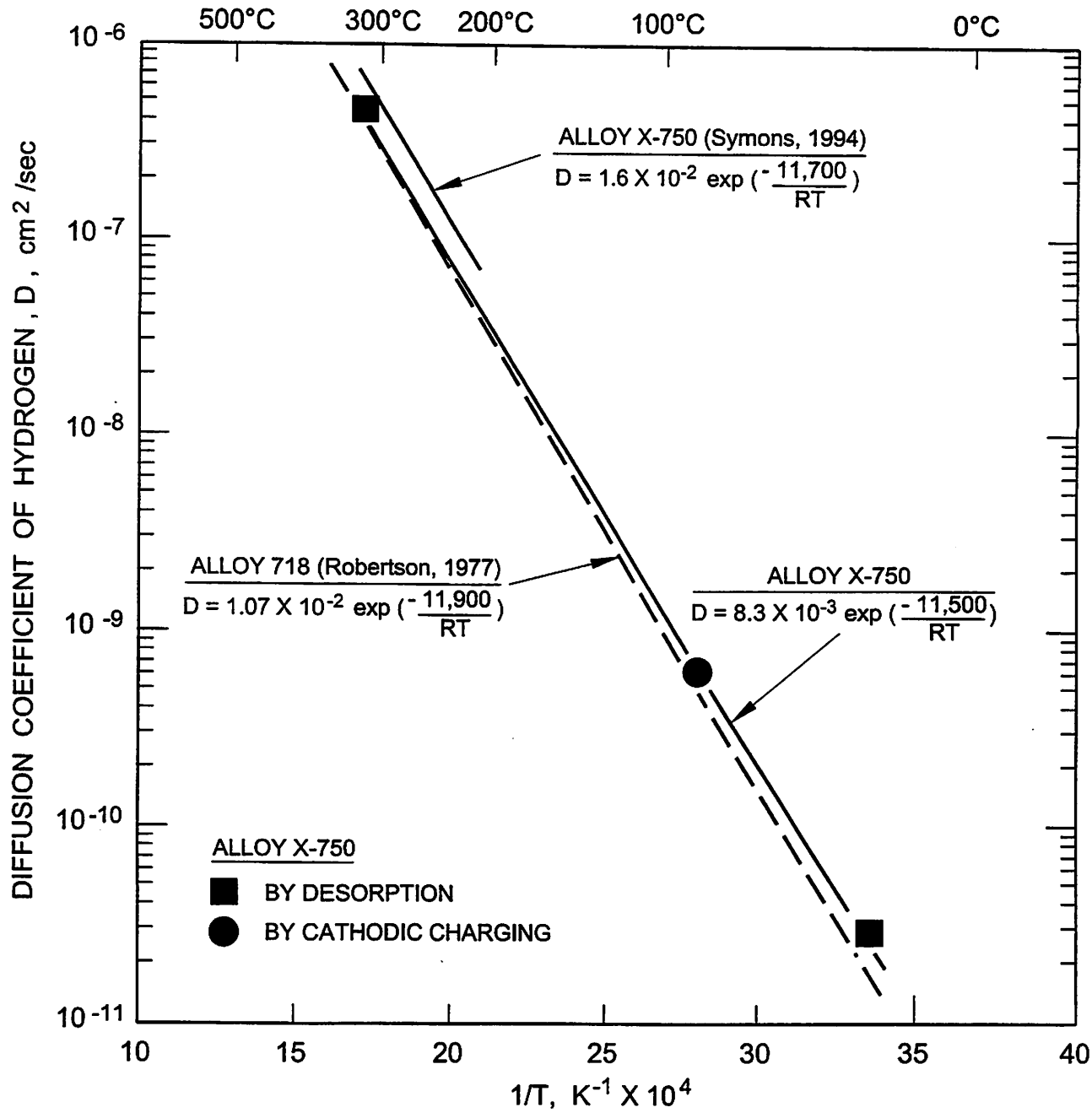

Figure 10. Comparison of hydrogen diffusion coefficients in Alloy X-750 and Alloy 718. (R=1.987 cal K^{-1} mol^{-1})

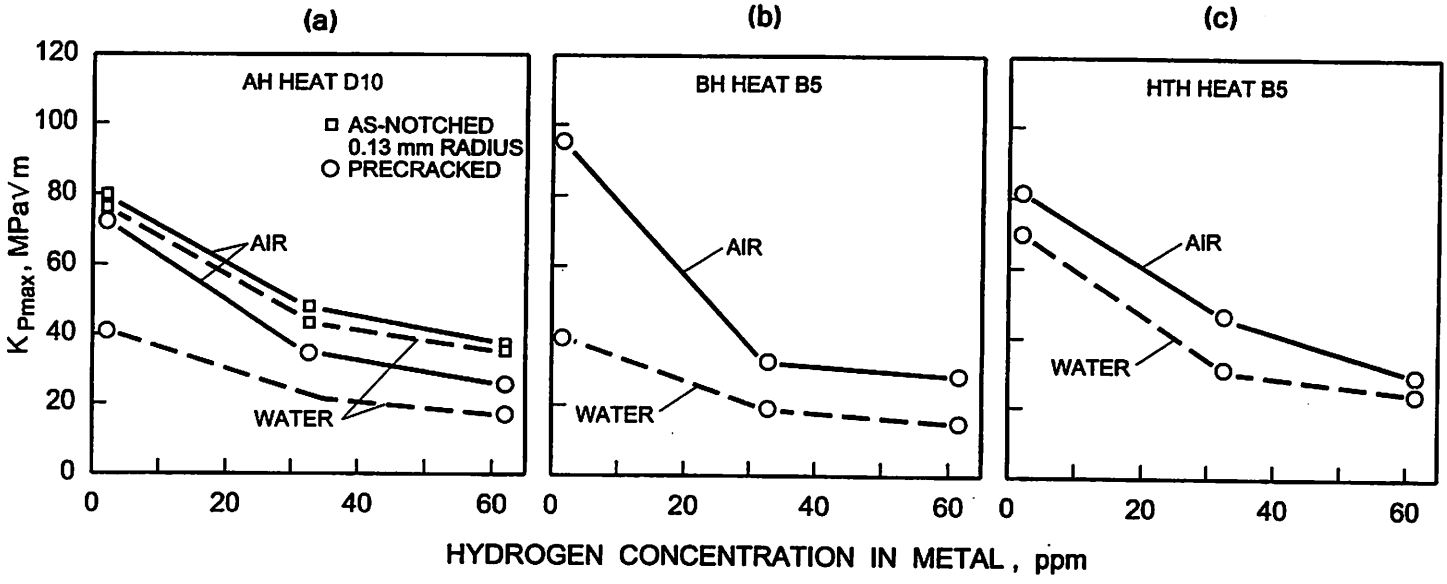

Figure 11. Individual and combined effects of precharged hydrogen and hydrogen picked up in low temperature water with 16 cc H_2/kg H_2O. AH specimens were tested in both the precracked and as-notched configurations. All BH and HTH specimens were precracked prior to testing.

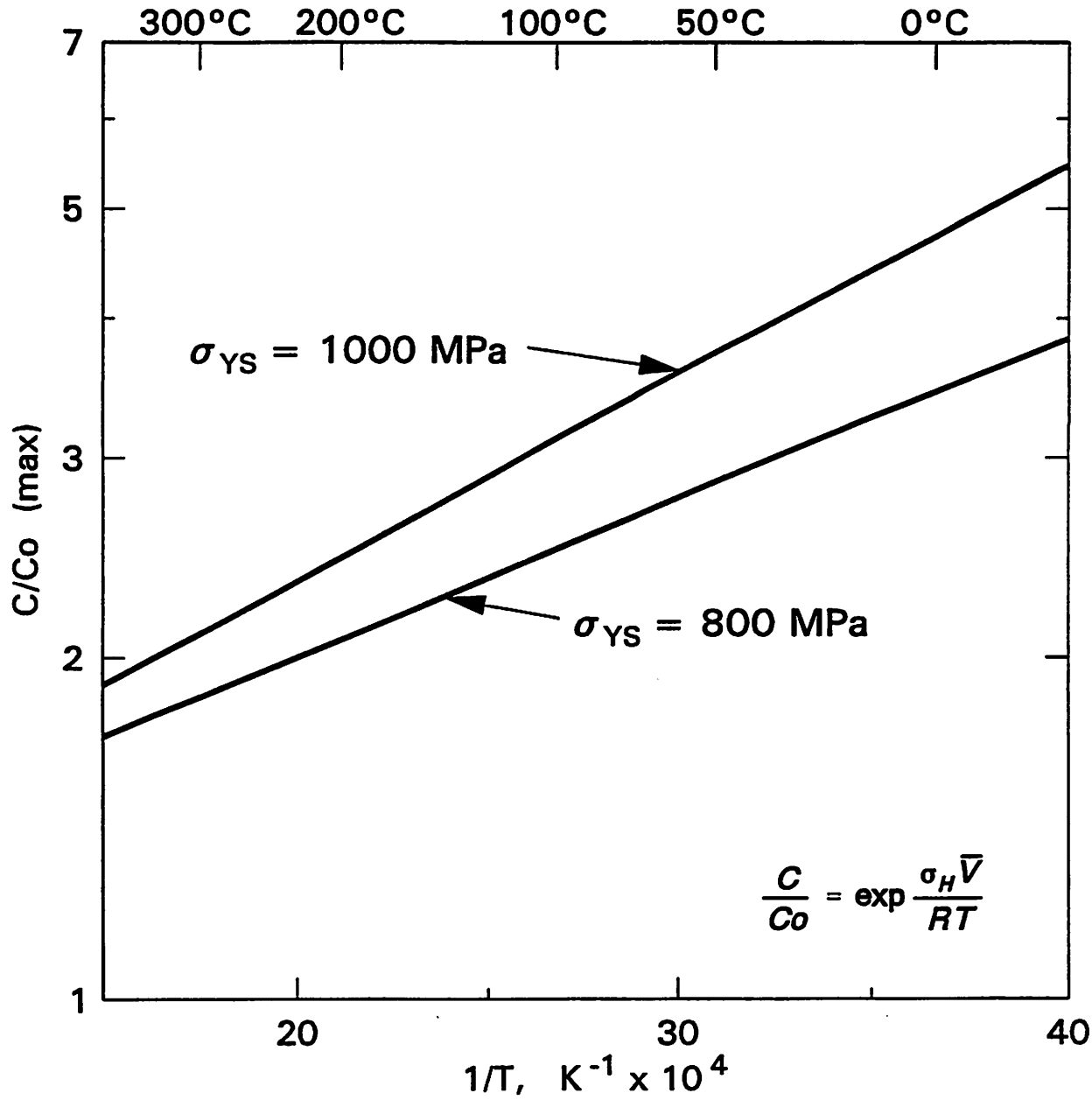

Figure 12. Effect of temperature and yield strength (σ_{YS}) on calculated maximum hydrogen enrichment in the peak triaxial stress region ahead of a crack in Alloy X-750.

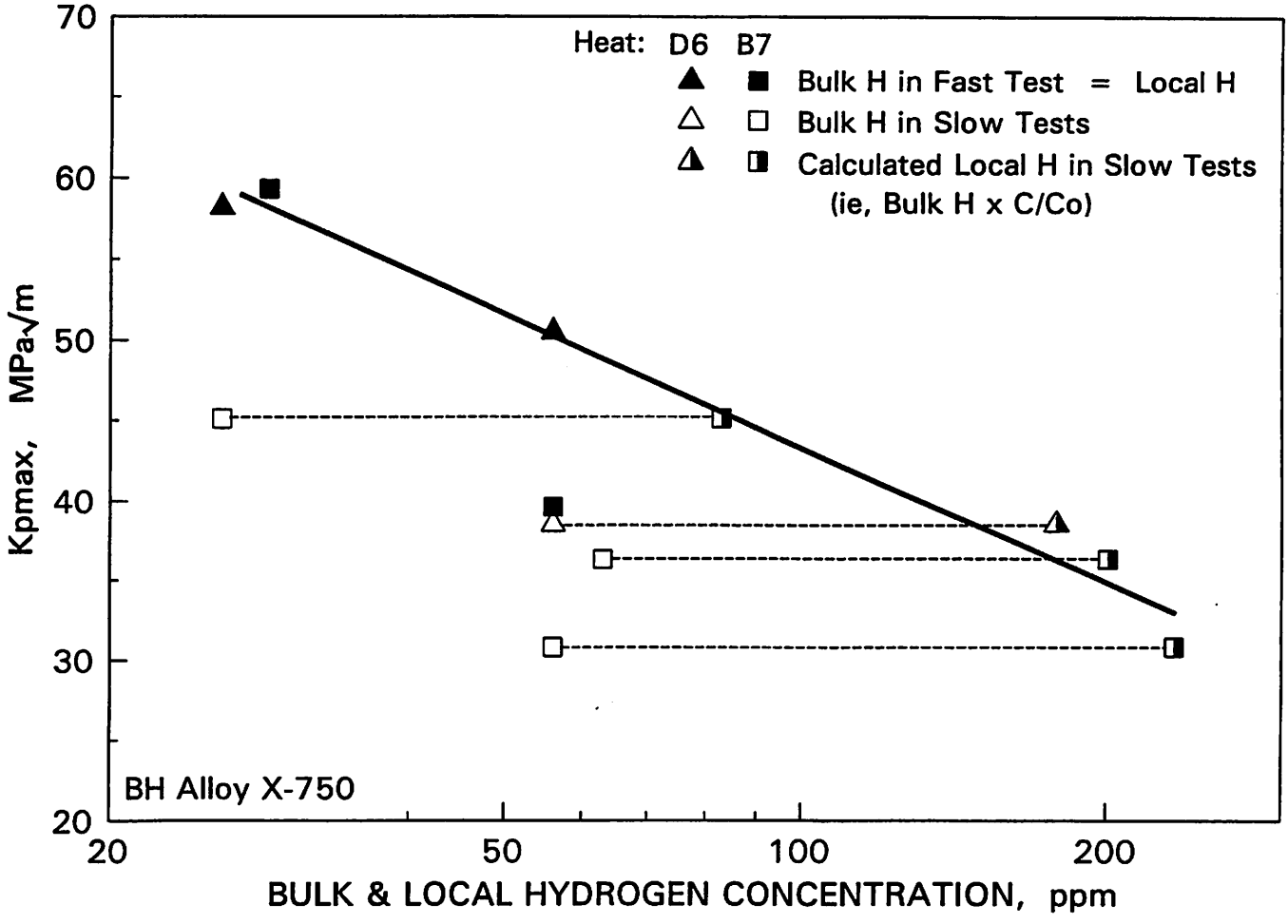

Figure 13. Hydrogen dependence of K_{Pmax} for precracked specimens from BH Heats B7 and D6 that were hydrogen precharged and tested in 24° and 93°C air. The solid line shows the correlation of K_{Pmax} with the measured bulk hydrogen content for fast tests (solid symbols) and calculated local hydrogen enrichment for slow tests (partially closed symbols). The low toughness exhibited in the fast test of the B7 specimen containing 56 ppm hydrogen is attributed to data scatter.

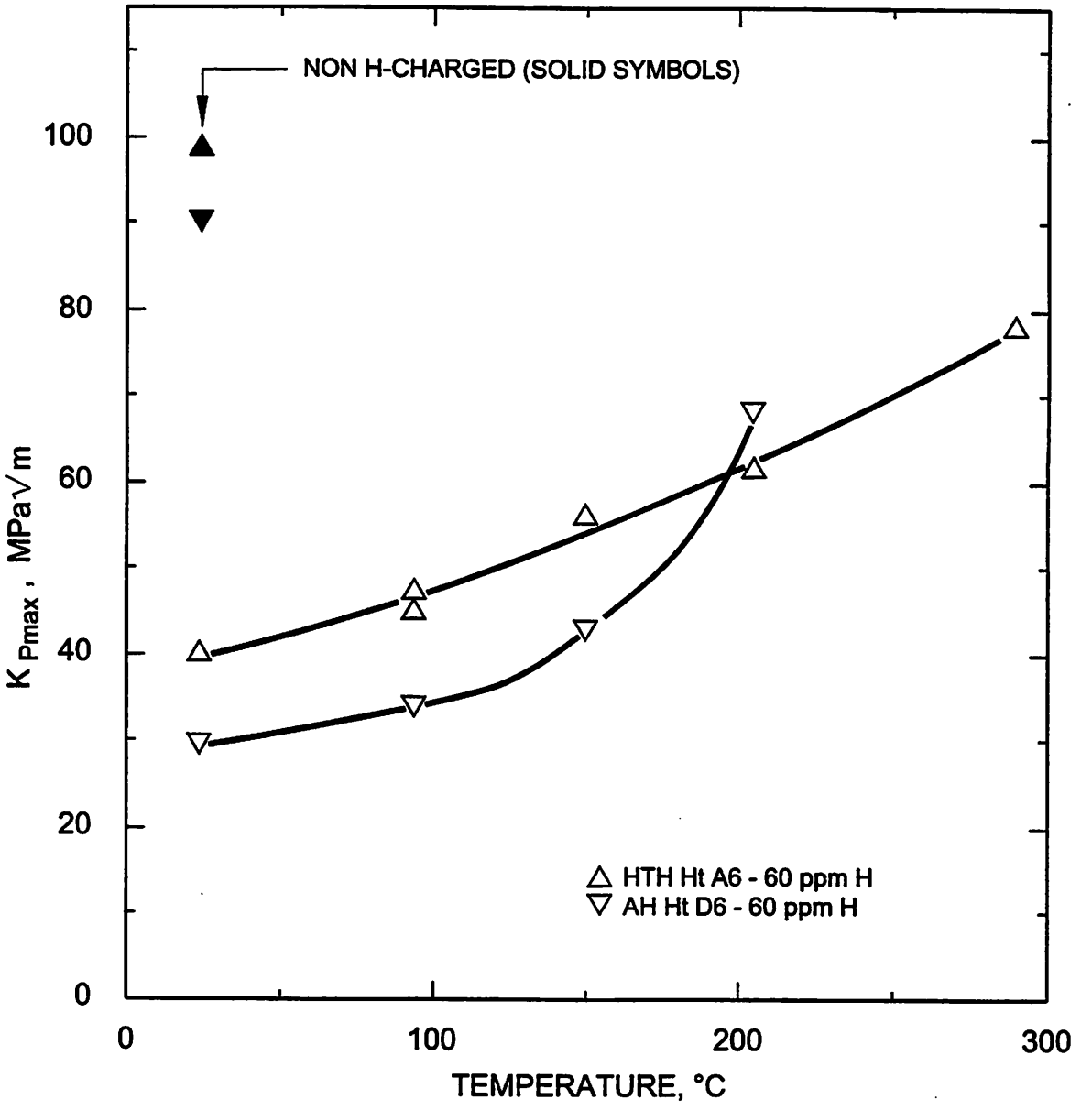

Figure 14. Temperature dependence of K_{Pmax} for precracked specimens that were hydrogen precharged and tested in air. Elevated temperature test times were minimized to preclude significant hydrogen loss.

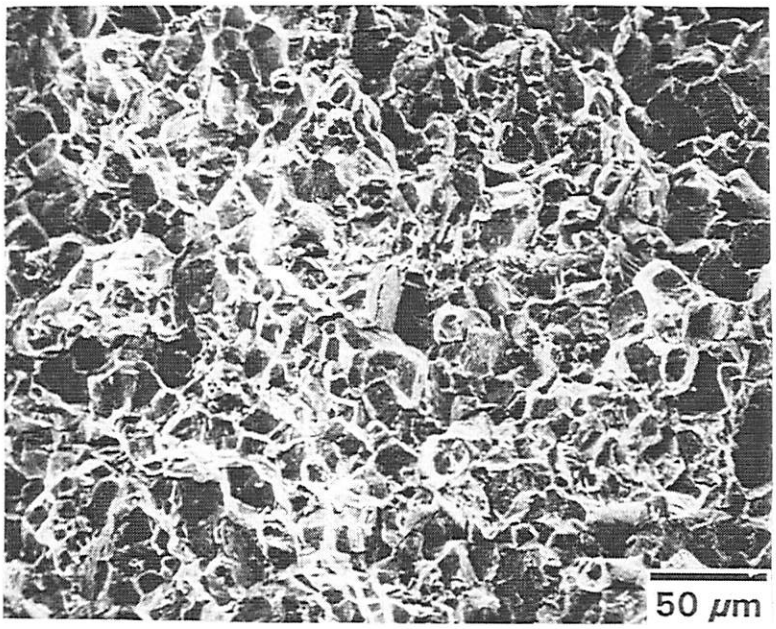

(a)

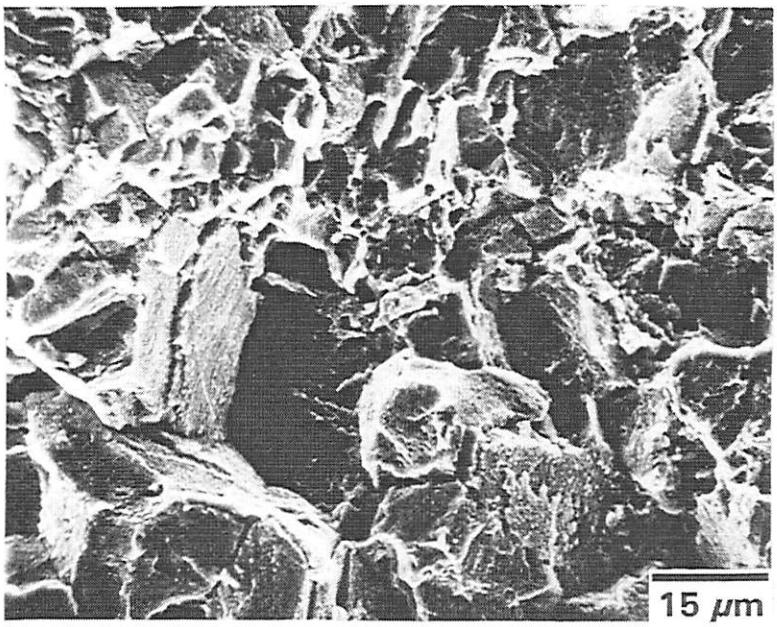

(b)

Figure 15. Fracture surface morphology for hydrogen-charged specimen tested in 288°C air.
(a) Mixed mode fracture with approximately equal amounts of intergranular and transgranular cracking.
(b) High magnification of center region of (a) showing transgranular facets associated with a channel fracture mechanism.

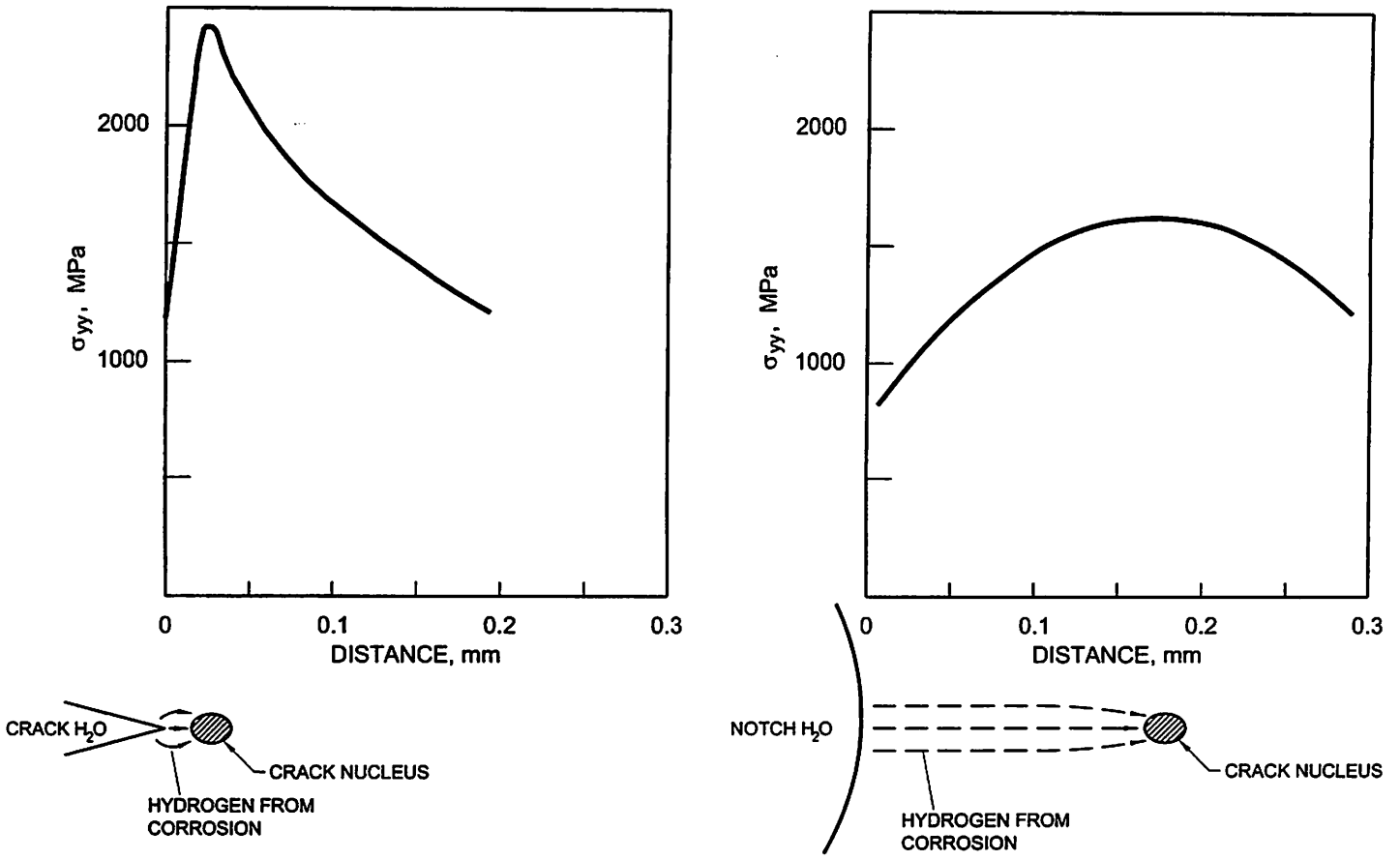

Figure 16. Illustration of difference in peak principal stress (σ_{yy}) and diffusion distance to assumed crack nucleation site for hydrogen released by corrosion reaction in precracked and as-notched specimens. Y direction is normal to the crack or notch plane.

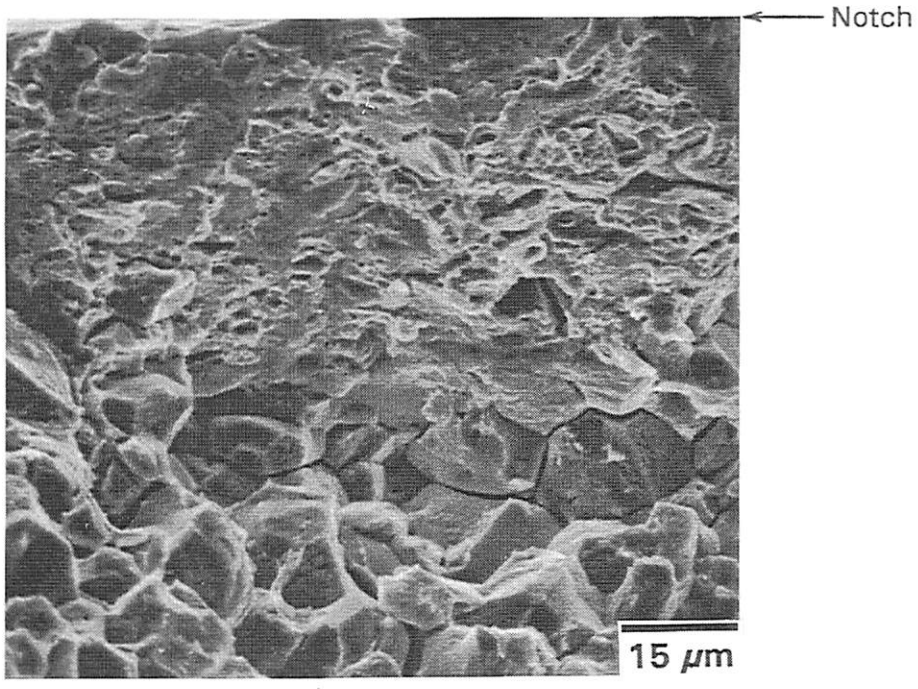

Figure 17. As-notched specimen from BH Heat B4 tested in 88°C water showing a transgranular dimple rupture region between base of notch and intergranular region.

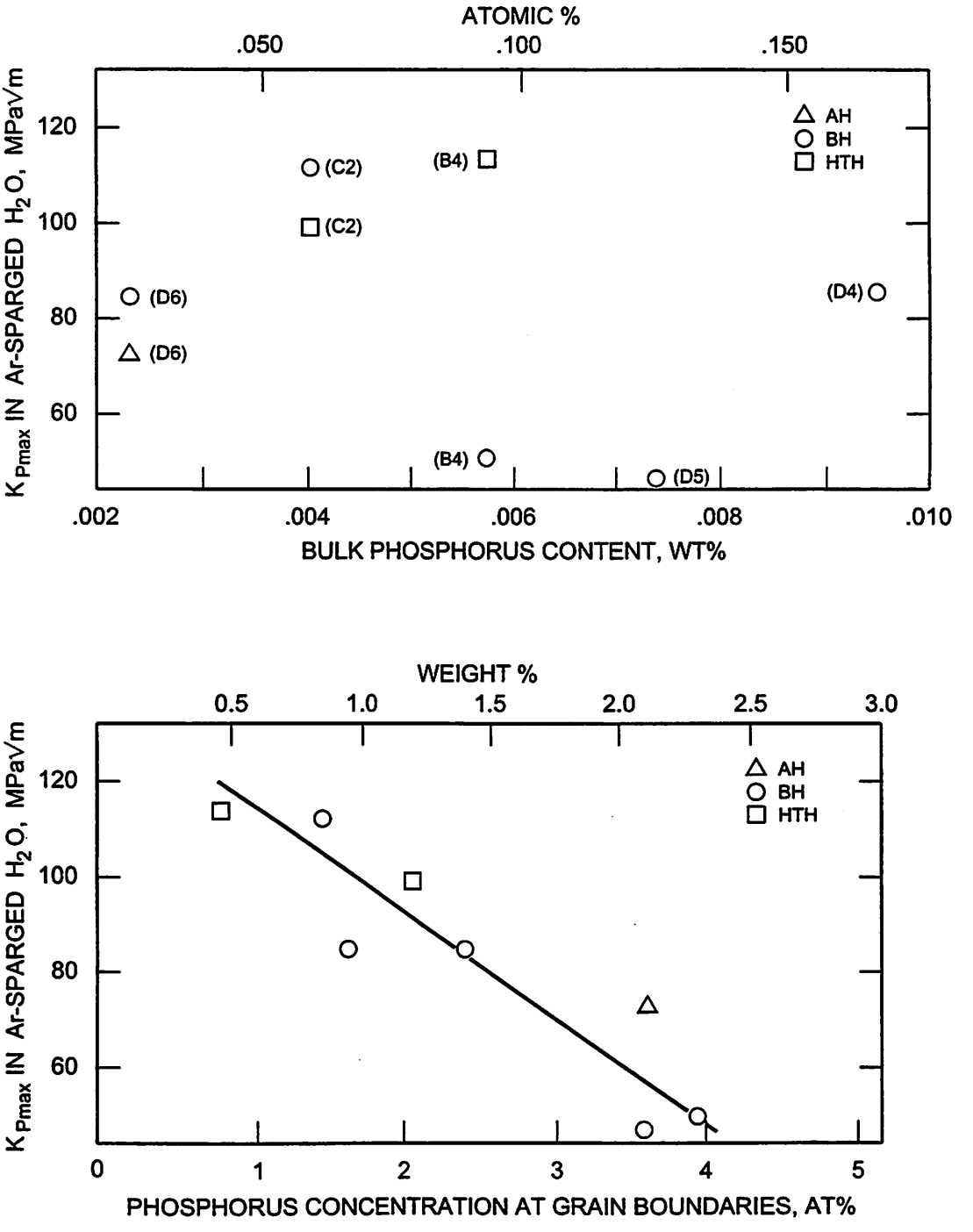

Figure 18. Correlation of rising load K_{Pmax} values in argon-sparged deionized water at 93°C with bulk and grain boundary phosphorus concentrations. LTCP resistance correlates with grain boundary phosphorus content, but not with bulk content. Heat identification is provided inside parenthesis.

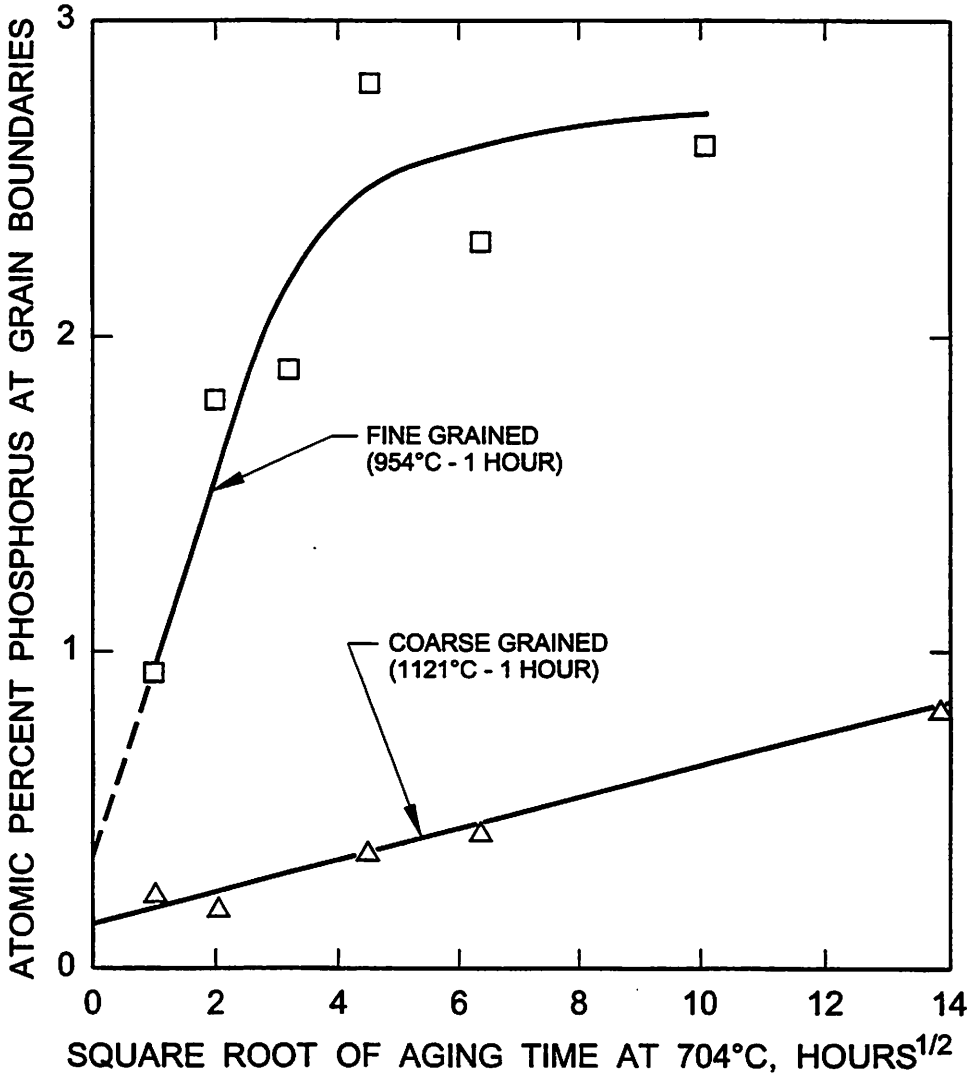

Figure 19. Phosphorus segregation kinetics at 794°C in coarse and fine grain samples from Heat B4. Prior to 704°C aging, the fine grain material was annealed at 954°C whereas a 1121°C anneal was used to produce a coarse grain structure.

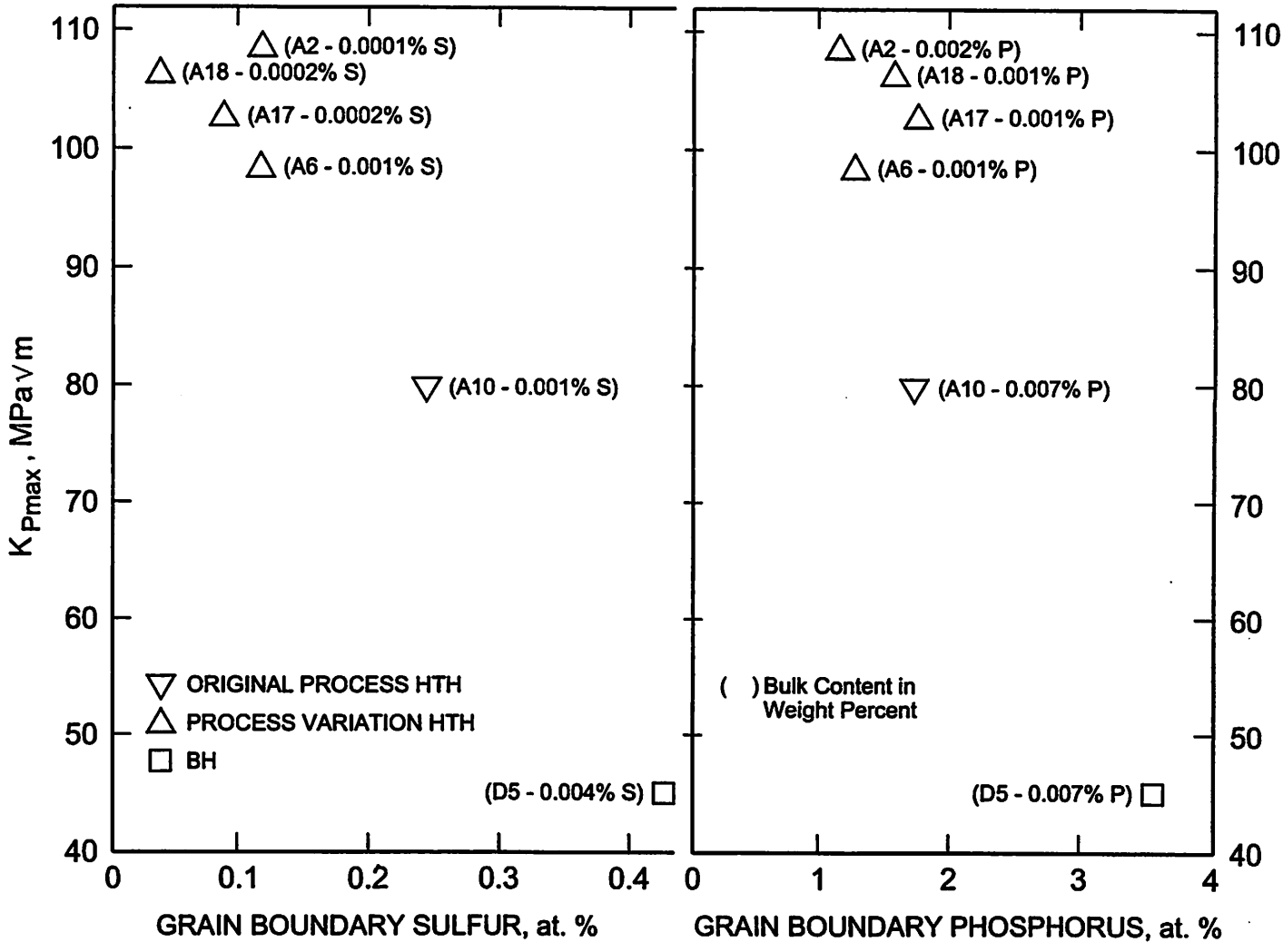

Figure 20. Correlation of rising load K_{Pmax} values in argon-sparged 93°C water with grain boundary sulfur and phosphorus concentrations. Grain boundary sulfur correlates with variability in K_{Pmax} values for BH and HTH heats. While lower grain boundary phosphorus accounts for the overall improvement in LTCP resistance for Condition HTH, it does not correlate with heat-to-heat variations. Heat identification and bulk sulfur and phosphorus contents are provided parenthetically.

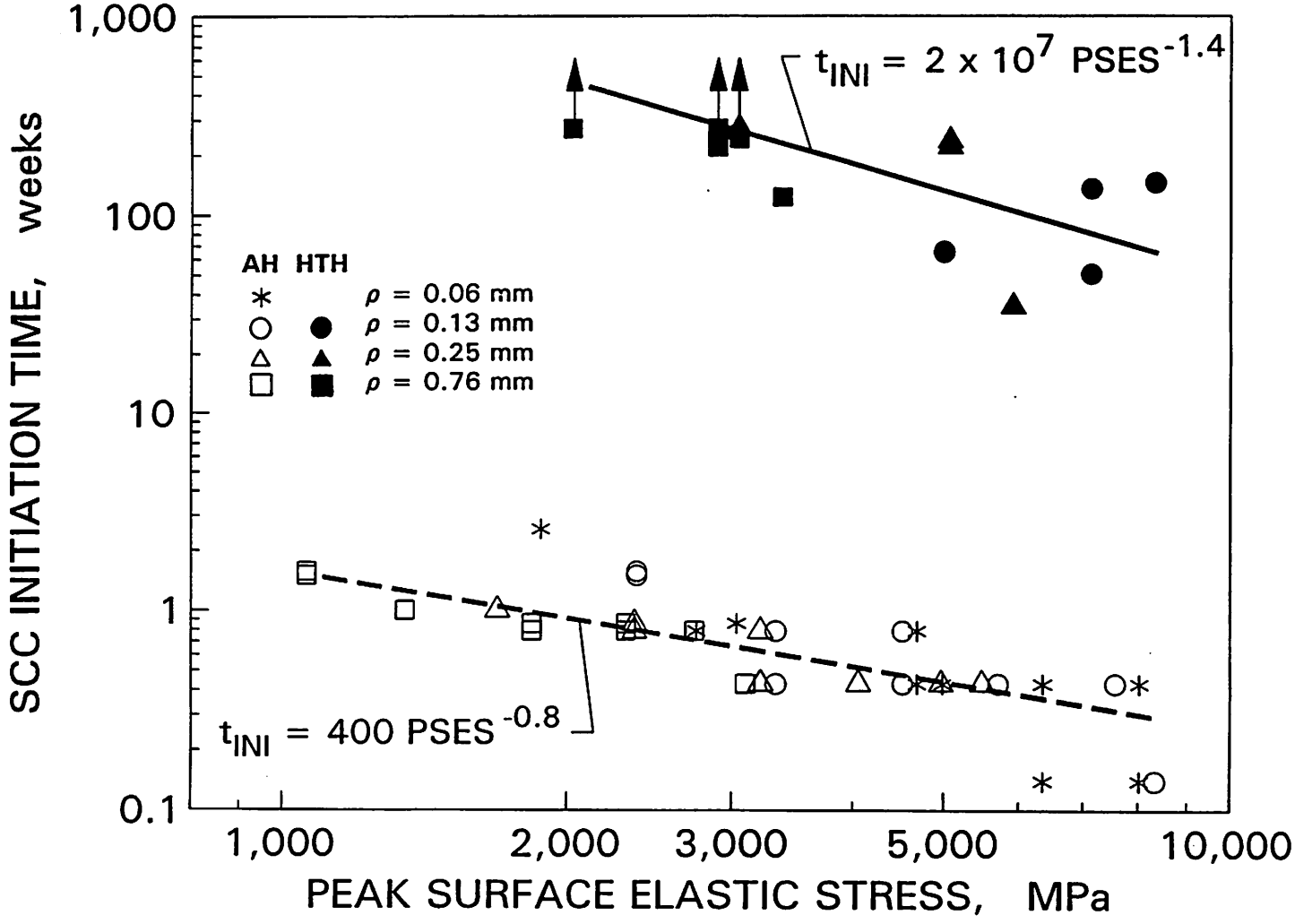

Figure 21. SCC initiation time in 360°C water as a function of PSES for as-notched CT specimens from AH Heat D8 and HTH Heat A6. Power-law correlations are based on maximum-likelihood analysis. Up arrows indicate absence of HTSCC.

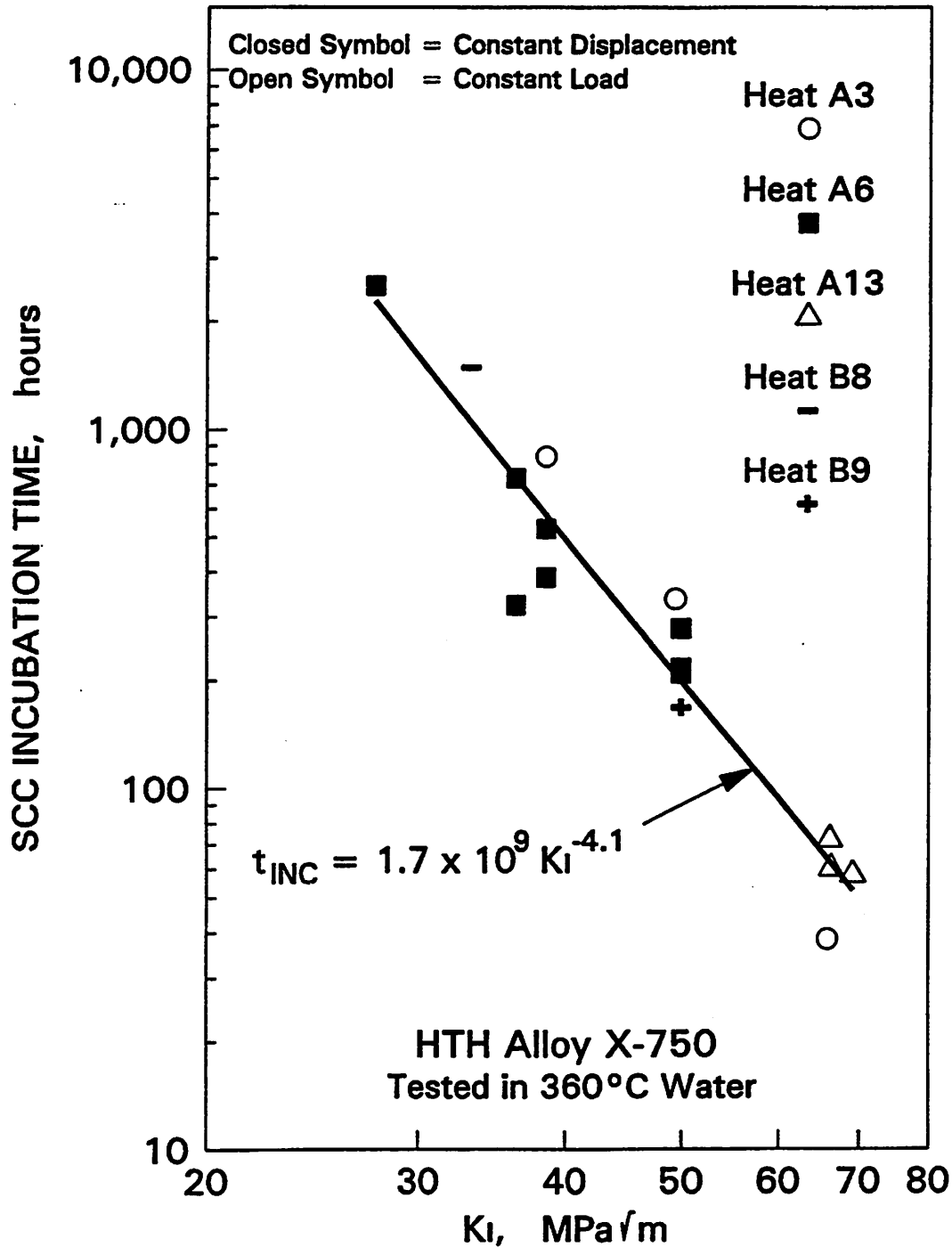

Figure 22. K_I dependence of SCC incubation times for precracked CT specimens for five HTH heats.

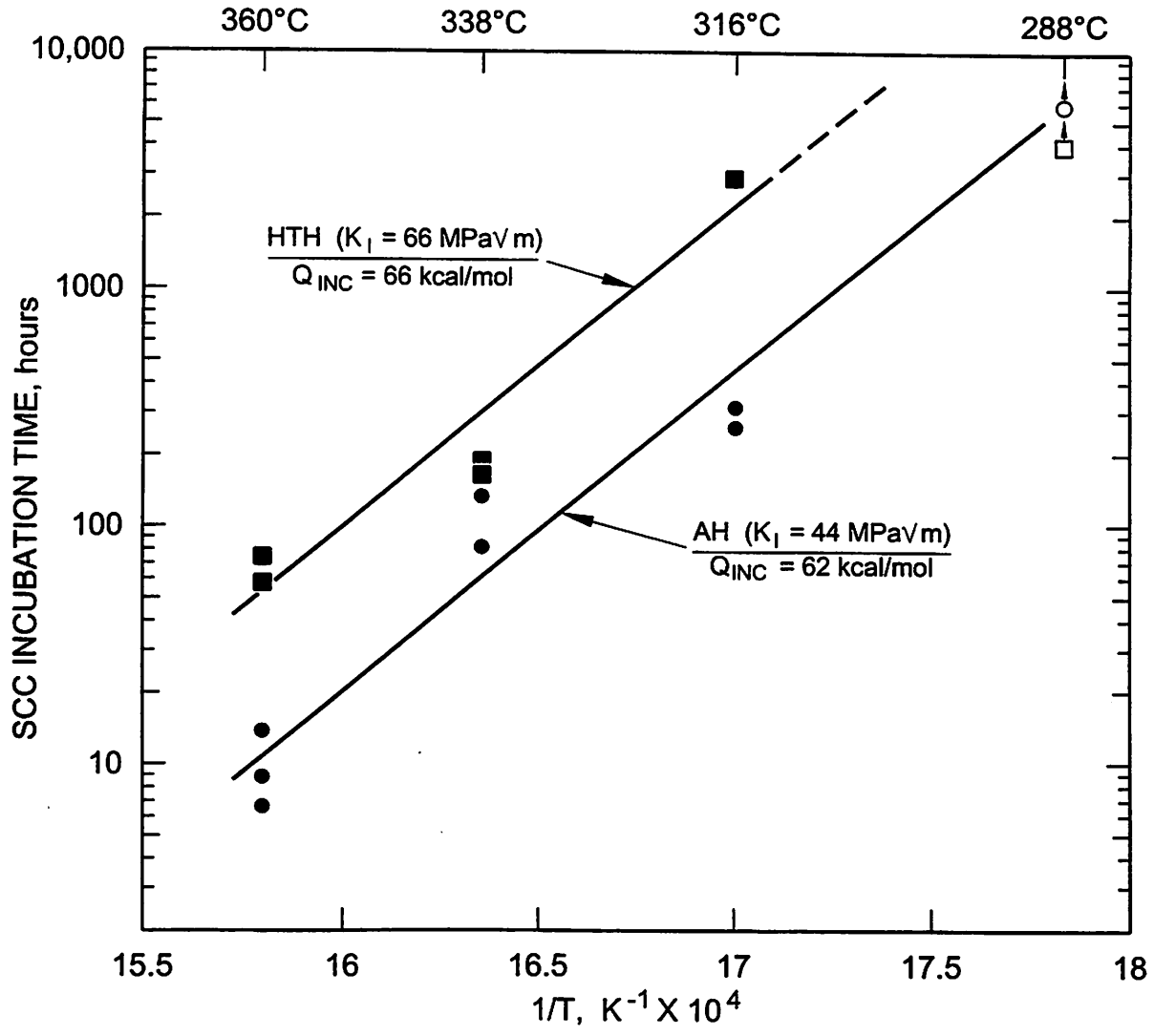

Figure 23. Temperature dependence of SCC incubation times for precracked CT specimens from AH Heat D9 and HTH Heat A13. Open symbols with arrows denote absence of HTSCC.

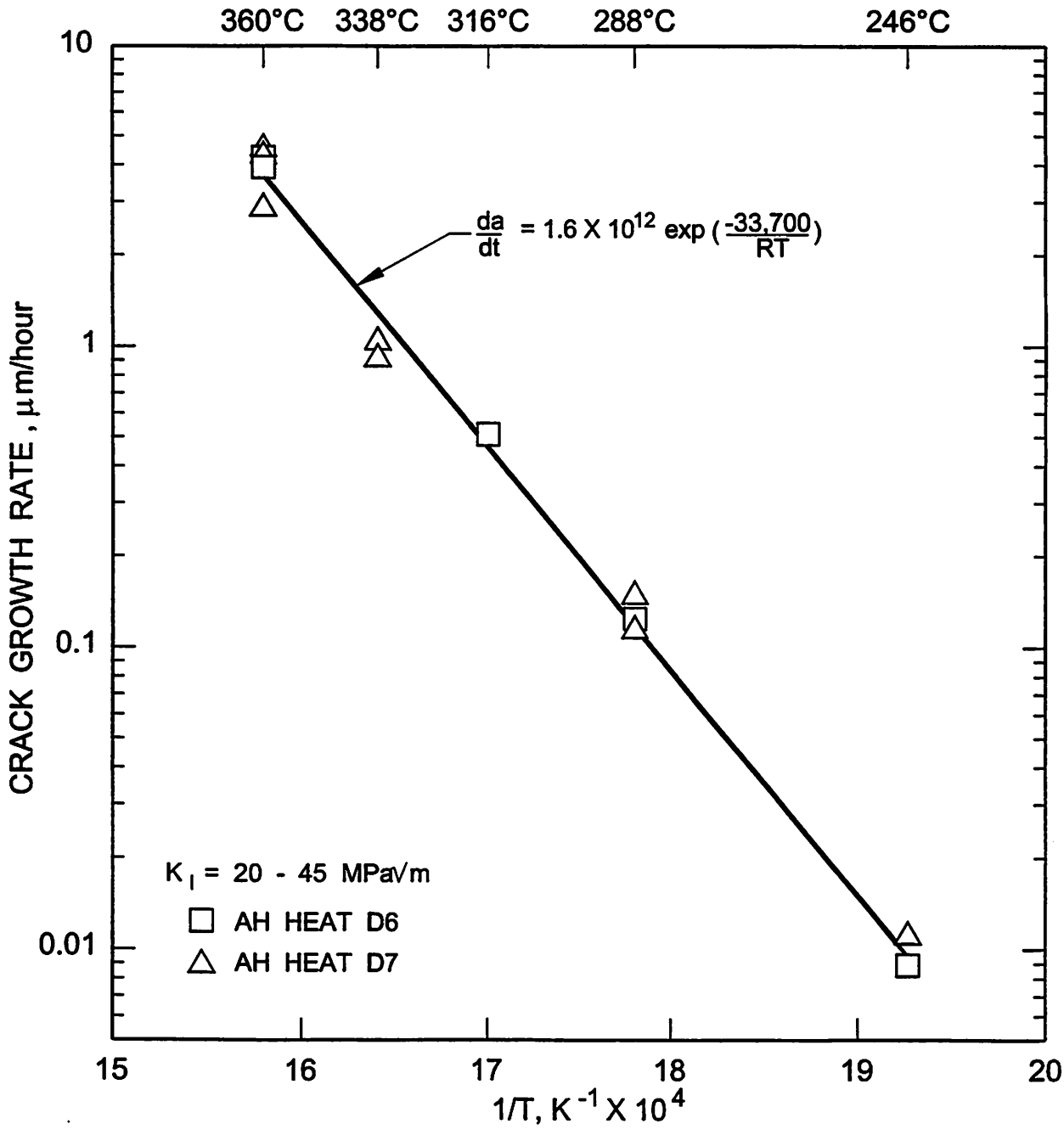

Figure 24. Arrhenius plot of Stage II SCC rates for Condition AH Heats D6 and D7.

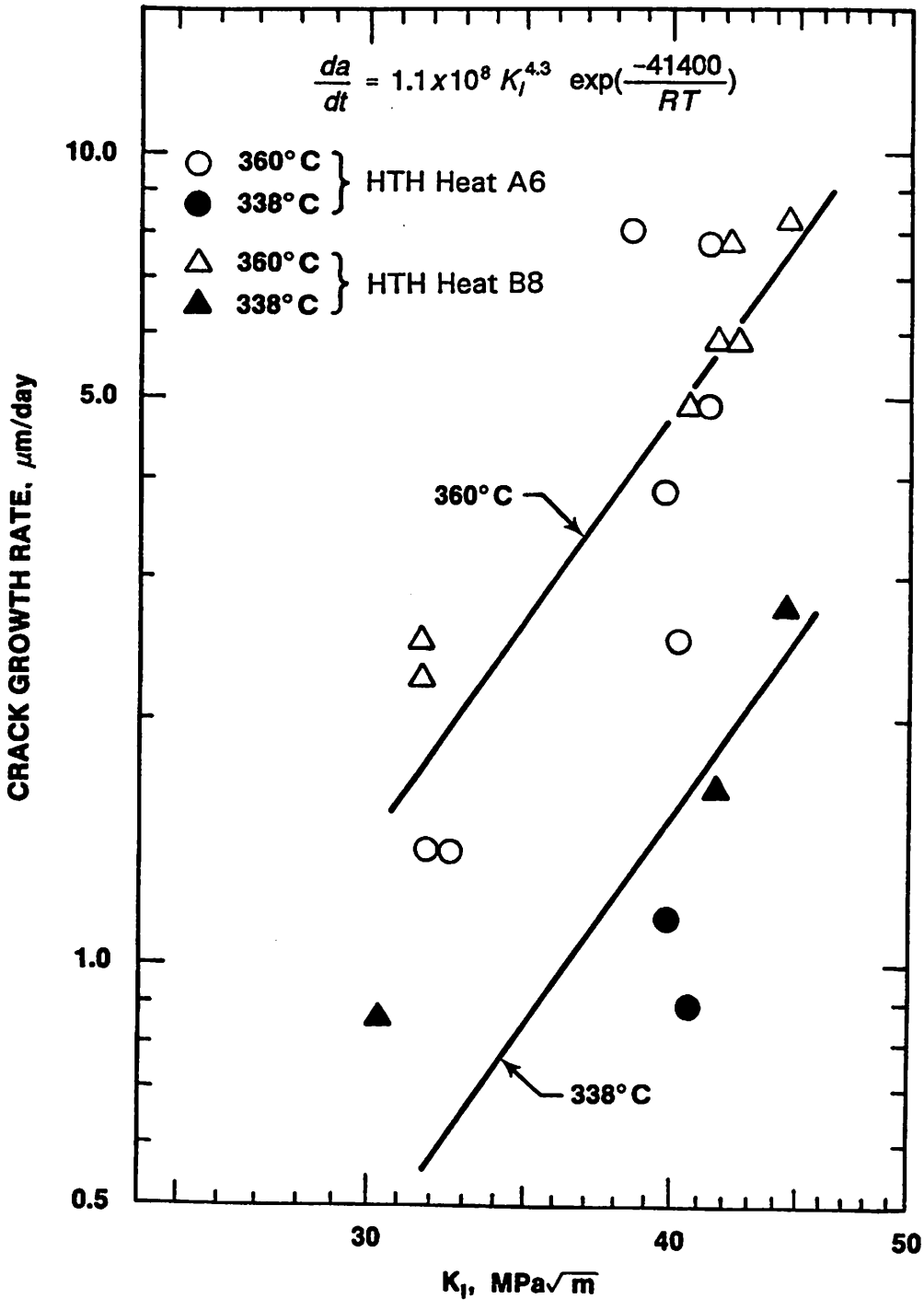

Figure 25. Temperature and K_I dependence of SCC rates for Condition HTH.

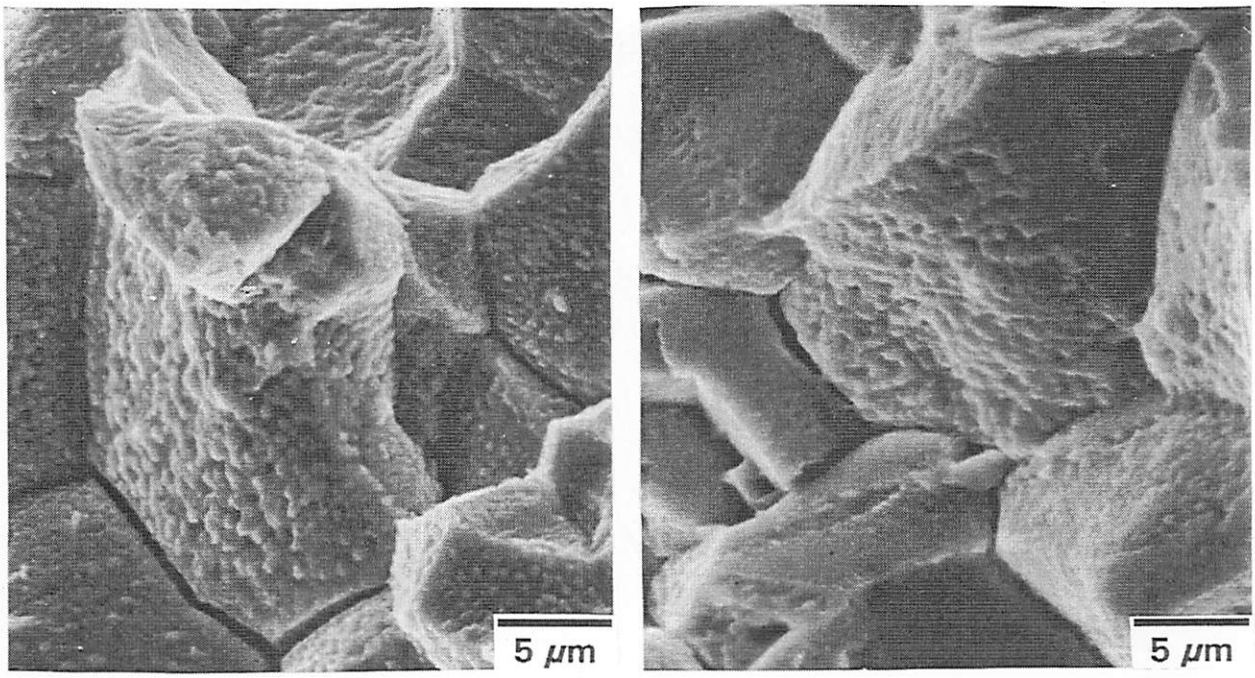

(a) (b)

Figure 26. Intergranular fracture surface morphologies associated with HTSCC and hydrogen-precharged specimen tested in air are indistinguishable.
(a) SCC fracture surface for BH Heat B6 tested in 360°C water.
(b) Fracture surface for hydrogen-charged BH Heat B6 tested in room temperature air.